UNIVERSITY OF THESSALY

SCHOOL OF ENGINEERING

DEPARTMENT OF ELECTRICAL AND COMPUTER ENGINEERING

Study and simulation of Brushless DC motor drive system

Diploma Thesis

Manola Varvara

Supervisor: Bargiotas Dimitrios

Volos 2020

UNIVERSITY OF THESSALY

SCHOOL OF ENGINEERING

DEPARTMENT OF ELECTRICAL AND COMPUTER ENGINEERING

Study and simulation of Brushless DC motor drive system

Diploma Thesis

Manola Varvara

Supervisor: Bargiotas Dimitrios

Volos 2020

ΠΑΝΕΠΙΣΤΗΜΙΟ ΘΕΣΣΑΛΙΑΣ

ΠΟΛΥΤΕΧΝΙΚΗ ΣΧΟΛΗ

ΤΜΗΜΑ ΗΛΕΚΤΡΟΛΟΓΩΝ ΜΗΧΑΝΙΚΩΝ ΚΑΙ ΜΗΧΑΝΙΚΩΝ ΥΠΟΛΟΓΙΣΤΩΝ

Μελέτη και προσομοίωση του κυκλώματος οδήγησης Brushless DC κινητήρα

Διπλωματική Εργασία

Μανώλα Βαρβάρα

Επιβλέπων: Μπαργιώτας Δημήτριος

Βόλος 2020

Εγκρίνεται από την Εξεταστική Επιτροπή:

Επιβλέπων **Μπαργιώτας Δημήτριος**

Αναπληρωτής Καθηγητής, Τμήμα Ηλεκτρολόγων Μηχανικών και Μηχανικών Υπολογιστών, Πανεπιστήμιο Θεσσαλίας

Μέλος **Τσομπανοπούλου Παναγιώτα**

Αναπληρώτρια Καθηγήτρια, Τμήμα Ηλεκτρολόγων Μηχανικών και Μηχανικών Υπολογιστών, Πανεπιστήμιο Θεσσαλίας

Μέλος **Τσουκαλάς Ελευθέριος**

Καθηγητής, Τμήμα Ηλεκτρολόγων Μηχανικών και Μηχανικών Υπολογιστών, Πανεπιστήμιο Θεσσαλίας

Ημερομηνία έγκρισης: Οκτώβριος 2020

ACKNOWLEDGEMENTS

I want to express my gratitude to my advisor, Prof. Dimitrios Bargiotas. This thesis would not have been possible without his guidance and help during this project.

Thank you to my friends for all the fun moments we have had together throughout these years. I will remember the nights working together before deadlines for the rest of my life. Special thanks to my best friend for always encouraging me and not letting me give up on my goal.

I owe my deepest gratitude to my parents whose unconditional love and financial support made it possible for me to complete my studies. I would also like to thank my brothers and sister for their understanding and support throughout my studies. I am blessed to having you as my family.

ΥΠΕΥΘΥΝΗ ΔΗΛΩΣΗ ΠΕΡΙ ΑΚΑΔΗΜΑΪΚΗΣ ΔΕΟΝΤΟΛΟΓΙΑΣ ΚΑΙ ΠΝΕΥΜΑΤΙΚΩΝ ΔΙΚΑΙΩΜΑΤΩΝ

Με πλήρη επίγνωση των συνεπειών του νόμου περί πνευματικών δικαιωμάτων, δηλώνω ρητά ότι η παρούσα διπλωματική εργασία, καθώς και τα ηλεκτρονικά αρχεία και πηγαίοι κώδικες που αναπτύχθηκαν ή τροποποιήθηκαν στα πλαίσια αυτής της εργασίας, αποτελεί αποκλειστικά προϊόν προσωπικής μου εργασίας, δεν προσβάλλει κάθε μορφής δικαιώματα διανοητικής ιδιοκτησίας, προσωπικότητας και προσωπικών δεδομένων τρίτων, δεν περιέχει έργα/εισφορές τρίτων για τα οποία απαιτείται άδεια των δημιουργών/δικαιούχων και δεν είναι προϊόν μερικής ή ολικής αντιγραφής, οι πηγές δε που χρησιμοποιήθηκαν περιορίζονται στις βιβλιογραφικές αναφορές και μόνον και πληρούν τους κανόνες της επιστημονικής παράθεσης. Τα σημεία όπου έχω χρησιμοποιήσει ιδέες, κείμενο, αρχεία ή/και πηγές άλλων συγγραφέων, αναφέρονται ευδιάκριτα στο κείμενο με την κατάλληλη παραπομπή και η σχετική αναφορά περιλαμβάνεται στο τμήμα των βιβλιογραφικών αναφορών με πλήρη περιγραφή. Αναλαμβάνω πλήρως, ατομικά και προσωπικά, όλες τις νομικές και διοικητικές συνέπειες που δύναται να προκύψουν στην περίπτωση κατά την οποία αποδειχθεί, διαχρονικά, ότι η εργασία αυτή ή τμήμα της δεν μου ανήκει διότι είναι προϊόν λογοκλοπής.

Η Δηλούσα

Μανώλα Βαρβάρα

Οκτώβριος 2020

ABSTRACT

The purpose of this diploma thesis is the study and the simulation of a Permanent Magnet Synchronous Motor – Brushless DC motor drive system. After the bibliographic review and the theoretical analysis of the research data in the first three chapters concerning the theoretical part of thesis, then two chapters follow with the experimental part of the work, where the operation of the BLDC motor is simulated. More specifically, the advantages of BLDC motor compared to other types of motors are presented, emphasizing their use in a variety of applications. Then, the structural characteristics of the motor are analyzed, which indicates the absence of brushes in the stator and the capability of rotor movement using permanent magnets. Also, the operation principle of the BLDC motor is described, either by using Hall sensors to detect the rotor position or by using sensorless methods. Moreover, the subsystems that constitute the complete motor drive system are analyzed. Then follows the experimental part, where the Simulink/Matlab environment is used to model the closed loop speed control system and simulate the motor operation. The structure of the model is focused on the development of subsystems which compose the complete motor drive system. To explain the position of each subsystem in the complete system, its operation is described and the input and output of each subsystem are clarified. The use of subsystems is related to the individual control systems, and is aimed to make it easier to manage and flexibly alter the complete system. The simulation experiment involves the motor response to both speed alterations and mechanical load application. The simulation results are presented to waveforms that demonstrate the proper operation of the motor drive system.

ΠΕΡΙΛΗΨΗ

Στην παρούσα διπλωματική εργασία πραγματοποιείται η μελέτη καθώς και προσομοίωση του κυκλώματος οδήγησης ενός Σύγχρονου Κινητήρα Μονίμου Μαγνήτη τύπου Brushless. Αφού γίνει η βιβλιογραφική ανασκόπηση και παρατεθεί η θεωρητική ανάλυση των στοιχείων της έρευνας στα τρία πρώτα κεφάλαια που αφορούν το θεωρητικό κομμάτι της εργασίας, στη συνέχεια ακολουθούν δύο κεφάλαια με το πειραματικό κομμάτι της εργασίας, όπου προσομοιώνεται η λειτουργία του κινητήρα BLDC. Πιο αναλυτικά, παρουσιάζονται τα πλεονεκτήματα των κινητήρων BLDC σε σύγκριση με άλλα είδη κινητήρων, τονίζοντας την ευρεία χρήση τους σε ποικίλες εφαρμογές. Στη συνέχεια, αναλύονται τα κατασκευαστικά χαρακτηριστικά του κινητήρα που υποδηλώνουν την απουσία ψηκτρών στο στάτη και τη δυνατότητα περιστροφής του δρομέα με χρήση μόνιμων μαγνητών. Ακόμη, επεξηγείται ο τρόπος λειτουργίας του με χρήση αισθητήρων θέσης αλλά και χωρίς τη χρήση αυτών. Επίσης, αναλύονται τα επιμέρους κυκλώματα που συναποτελούν το ολοκληρωμένο κύκλωμα οδήγησης του κινητήρα. Στη συνέχεια ακολουθεί το πειραματικό κομμάτι, όπου γίνεται η μοντελοποίηση του κυκλώματος ελέγχου ταχύτητας κλειστού βρόχου στο περιβάλλον του Simulink/Matlab, μέσω του οποίου προσομοιώνεται η λειτουργία του κινητήρα. Η δομή του μοντέλου βασίζεται στην δημιουργία υποσυστημάτων, τα οποία συνθέτουν το ολοκληρωμένο κύκλωμα οδήγησης του κινητήρα. Γίνεται περιγραφή της λειτουργίας των επιμέρους υποσυστημάτων και υπογραμμίζεται η είσοδος και η έξοδος κάθε υποσυστήματος, ώστε να διευκρινιστεί ο ρόλος τους στο σύνολο του κυκλώματος. Η χρήση υποσυστημάτων ισοδυναμεί με την απομόνωση των επιμέρους κυκλωμάτων ελέγχου και αποσκοπεί τόσο στην εύκολη διαχείριση του συνολικού κυκλώματος, όσο και στην ευέλικτη τροποποίησή του. Το πείραμα της προσομοίωσης περιλαμβάνει την απόκριση του κινητήρα τόσο σε αλλαγές της ταχύτητας όσο και μετά την επιβολή μηχανικού φορτίου. Τα αποτελέσματά της παρουσιάζονται μέσω γραφικών παραστάσεων στις οποίες μελετάται, και εν τέλει επιβεβαιώνεται, η σωστή λειτουργία των επιμέρους κυκλωμάτων.

CONTENTS

LIST OF FIGURES

LIST OF TABLES

CHAPTER 1

INTRODUCTION

Advancements in solid state technology in the early 1960s resulted in the invention of the first brushless DC (BLDC) motor in 1962, what T.G. Wilson and P.H. Trickey called a “DC machine with solid state commutation”. A brushless DC motor (also known as a BLDC motor or BL motor) is an electronically commutated DC motor with no brushes. It is similar to a permanent magnet synchronous motor.

BLDC motor is driven by DC voltage but current commutation is achieved by solid state switches. It has a permanent magnet for a rotor, and a three phase stator winding. Permanent magnets rotate around a fixed armature and overcome the problem of connecting current to the armature. Since the BLDC motor's rotor does not use coils, there is no need to supply it with current. That's why there are no brushes. However, BLDC motors are more difficult to drive than brushed motors.

There are three classifications of the BLDC motor: single-phase, two-phase and three-phase. The stator for each type has the same number of windings. The single-phase and three-phase motors are the most widely used. BLDC motors feature high efficiency and excellent controllability, and are widely used in many applications. They are available in many different power ratings, from very small motors as used in computer peripherals (disk drivers, printers) to larger motors used in electric cars. Furthermore, BLDC motor has power-saving advantages relative to other motor types.

BLDC motors are self-starting because the angle between the magnetic field of the rotor and the stator is fixed by the design of the motor. As a consequence, when power is applied the rotor is trying to turn towards the field of the stator from the very beginning. Speed of a brushless dc motor can be controlled by controlling the input DC voltage/current. Many different control algorithms have been used to provide control of BLDC motors.

The aim of this diploma thesis is to study the response of the BLDC simulation model. The simulation is implemented in Simulink/Matlab® environment. Simulink is a MATLAB-based

graphical programming environment for modeling, simulating and analyzing multidomain dynamical systems. Its primary interface is a graphical block diagramming tool and a customizable set of block libraries. It offers tight integration with the rest of the MATLAB environment and can either drive MATLAB or be scripted from it. Simulink is widely used in automatic control and digital signal processing for multidomain simulation and model-based design.

Chapter 2 presents the BLDC motor operation and the construction features of the motor. The mathematical model of BLDC motor is analyzed. And, also, describes some of the methods which are implemented in BLDC sensorless drive systems.

Chapter 3 contains the description of subsystems which constitute the complete motor drive system.

Chapter 4 presents the simulation model, as it is implemented in Simulink/Matlab® environment. The complete motor drive system consists of subsystems. The function of each subsystem is described analyzing the connection between subsystems.

Chapter 5 introduces the simulation results. The motor setting parameters and the output of each subsystem are presented. The study of model response is done through waveforms in which we can observe the model reaction to input alterations, during the simulation test.

Finally, the conclusion section contains the summary of this thesis and some projects for further work in the future.

CHAPTER 2

PERMANENT MAGNET SYNCHRONOUS MOTOR – BLDC MOTOR

2.1 Εισαγωγή

Brushless Direct Current (BLDC) motors are gaining prominence primarily due to their improved characteristics and efficiency on the other electric motors. There is a wide application of BLDC motors in industries, such as automotive, aerospace, medical, industrial automation and electric vehicles, due to its energy-efficient consumption. Furthermore, the BLDC motor has many advantages, such as power factor, low maintenance, and less rotor inertia. The popularity of BLDC motors is owed to their better efficiency, high power factor, high torque, less rotor inertia, easy control and longer life. The major disadvantage with permanent magnet motors is their higher value and relatively higher complexity caused by the power electronic converter which is used to drive them. [1], [2], [3], [4]

2.1.1 Comparing BLDC motors to other motor types

Based on the type of Back-EMF (electromotive force) waveform permanent magnet synchronous motors can be distinguished in two different kinds. The one with the trapezoidal Back-EMF waveform is called Brushless Direct Current (BLDC) motor and the other with the sinusoidal back-EMF is named Permanent Magnet Synchronous Motor (PMSM). The PMSM produce almost zero torque ripples, which offers higher efficiency. The power density in BLDC motor is 15% more than PMSM's, supposing that the copper losses are equal for both motors. In order to achieve the same torque the PMSM is more demanding than BLDC about current handling. [5] The differences between the BLDC motor and the PMSM are summarized in Table 2.1. [5]

Table 2.1 Comparison of BLDC and PMSM

	BLDC	PMSM
Winding Distribution	Trapezoidal	Sinusoidal
Energized Phase	Two Phases	Three Phases
Back-EMF Waveform	Trapezoidal	Sinusoidal
Torque Strength	Strong	Weak

BLDC motors have numerous benefits and few drawbacks opposed to Brushed DC motors and Induction motors. BLDC motors demand lower maintenance and as a result they last longer than Brushed DC motors. Also BLDC motors provide a bigger amount of output power per frame. Since the rotor is composed of permanent magnets, the rotor inertia is not as great as in other kind of motors. This increases the properties of acceleration and deceleration, which is shortening the operating cycles. Furthermore, their linear speed/torque characteristics enable foreseeable speed adjustment. By using BLDC motors, brush check is eradicated, that is making them the best option for restricted access areas and applications where service is complicated. Moreover, Brushed DC motors generate more noise than BLDC while operation, causing Electromagnetic Interference (EMI).

The high power to weight ratio, high torque, efficient dynamic control for variable speed applications, lack of brushes and commutator make the BLDC motor ideal for high performance applications. There is no mechanical wear of the moving parts due to the lack of brushes and commutator. Improved heat dissipation properties and high speeds operation enable them to be comparable to the typical DC motors. [6]

Table 2.2 summarizes the comparison between a BLDC motor and an Induction motor. Table 2.3 compares a BLDC motor to a Brushed DC motor. [7]

Table 2.2 Comparing a BLDC motor to an Induction motor

Features	BLDC Motors	AC Induction Motors
Speed/Torque Characteristics	Flat – Enables operation at all speeds with rated load.	Nonlinear – Lower torque at lower speeds.
Output Power/ Frame Size	High – Since it has permanent magnets on the rotor, smaller size can be achieved for a given output power.	Moderate – Since both stator and rotor have windings, the output power to size is lower than BLDC.
Rotor Inertia	Low – Better dynamic characteristics.	High – Poor dynamic characteristics.
Starting Current	Rated – No special starter circuit required.	Approximately up to seven times of rated – Starter circuit rating should be carefully selected. Normally uses a Star-Delta starter.
Control Requirements	A controller is always required to keep the motor running. The same controller can be used for variable speed control.	No controller is required for fixed speed; a controller is required only if variable speed is desired.
Slip	No slip is experienced between stator and rotor frequencies.	The rotor runs at a lower frequency than stator by slip frequency and slip increases with load on the motor.

Table 2.3 Comparing a BLDC motor to a Brushed DC motor

Feature	BLDC Motor	Brushed DC Motor
Commutation	Electronic commutation based on Hall position sensors.	Brushed commutation.
Maintenance	Less required due to absence of brushes.	Periodic maintenance is required.
Life	Longer.	Shorter.
Speed/Torque Characteristics	Flat – Enables operation at all speeds with rated load.	Moderately flat – At higher speeds, brush friction increases, thus reducing useful torque.
Efficiency	High – No voltage drop across brushes.	Moderate.
Output Power/ Frame Size	High – Reduced size due to superior thermal characteristics. Because BLDC has the windings on the stator, which is connected to the case, the heat dissipation is better.	Moderate/Low – The heat produced by the armature is dissipated in the air gap, thus increasing the temperature in the air gap and limiting specs on the output power/frame size.
Rotor Inertia	Low, because it has permanent magnets on the rotor. This improves the dynamic response.	Higher rotor inertia which limits the dynamic characteristics.
Speed Range	Higher – No mechanical limitation imposed by brushes/commutator.	Lower – Mechanical limitations by the brushes.
Electric Noise Generation	Low.	Arcs in the brushes will generate noise causing EMI in the equipment nearby.
Cost of Building	Higher – Since it has permanent magnets, building costs are higher.	Low.
Control	Complex and expensive.	Simple and inexpensive.
Control Requirements	A controller is always required to keep the motor running. The same controller can be used for variable speed control.	No controller is required for fixed speed; a controller is required only if variable speed is desired.

2.2 BLDC construction

BLDC motors usually have a cylindrical shape which is included from two pieces. The stable part which is named stator and the rotating part called rotor. Commonly rotor exists inside the stator. This type of construction enables the connection of the motor with all the systems which are needed to operate the motor. Also, restricting the rotor within the stator offers a natural cover to secure the rotating part from its surroundings. [8]

2.2.1 Stator

The stator is composed of stacked layering made of steel with windings positioned in the slots that are sliced along the axis at the inside of the stator, as shown in Figure 2.1. Most BLDC motors are connected in star with three stator windings. Each of these windings is created with numerous interconnected coils to construct a winding. One or more coils are inserted into the slots. Each of these windings is allocated over the inside of the stator to create an even number of poles. [7]

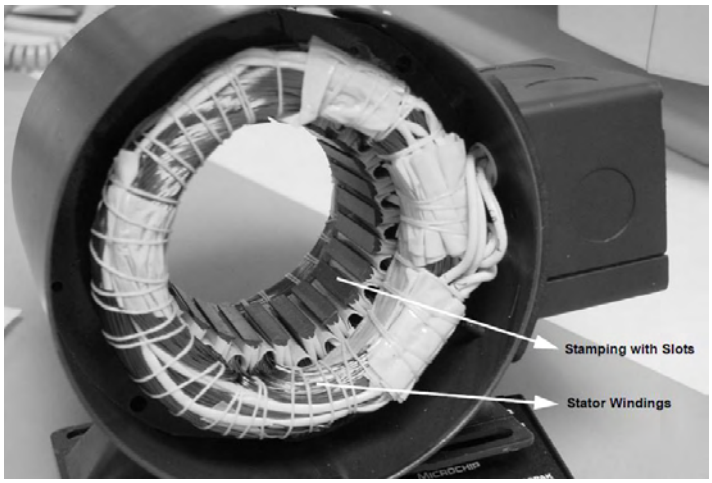

Figure 2.1 Stator

There are two versions of permanent magnet synchronous motors based on how the coils are connected in the stator windings and at the same time based on the form of induced voltage (BEMF - Back Electromotive Force). Therefore, the distinction is made on trapezoidal permanent magnet motors with trapezoidal BEMF (Figure 2.2) and sinusoidal permanent motors with sinusoidal BEMF (Figure 2.3). Also, the phase currents have a trapezoidal or sinusoidal figure, depending on the type of the motor. As a result, the torque on a sinusoidal machine is more stable than that of a trapezoidal machine. However, additional cost is required due to the complex connection of the windings to the sinusoidal motors because of the distribution of the windings in the stator. [7]

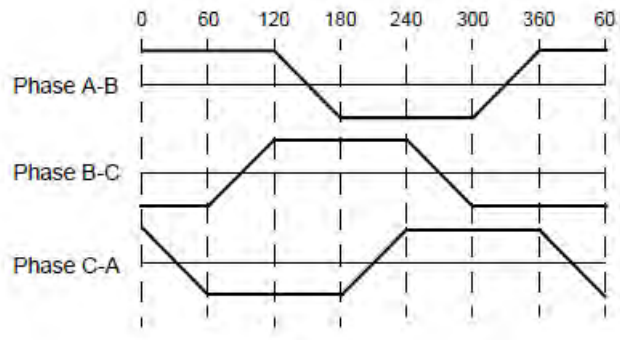

Figure 2.2 Trapezoidal BEMF

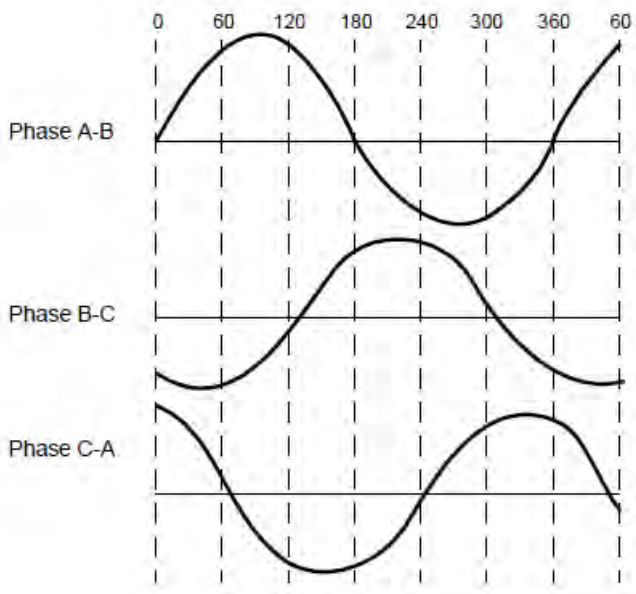

Figure 2.3 Sinusoidal BEMF

2.2.1.1 Hall effect sensors

In a BLDC motor commutation is achieved electronically instead of using brushes like in Brushed DC motors. In order to drive a BLDC motor, a commutation circuit is required to energize the stator windings according to the rotor position. The rotation is achieved by following a specific sequence which indicates which windings should be energized. Rotor position can be obtained, most frequently, by Hall Effect sensors embedded into the stator. Commonly, BLDC motors use three Hall sensors which are placed every 120° into the stator. [9]

Hall sensors are operated on the Hall effect. According to this, when a current-carrying conductor is inside a magnetic field, a transverse force is exerted on the current carriers, pushing them to one side of the conductor and displaying a potential difference at its ends. Thus, the sensors can determine the position of the rotor by detecting changes in the magnetic field. These changes are due to the alternation of positive and negative magnetic poles that pass near the sensors during the rotation.

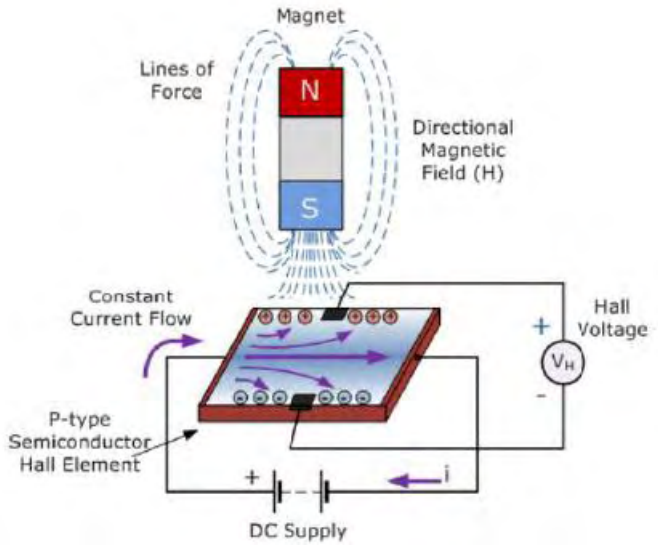

Figure 2.4 Representation of the Hall effect

More specifically, as shown in Figure 2.4, Hall sensors consist of a thin rectangular semiconductor material that is leaked from direct current. Once the semiconductor enters a magnetic field, Lorentz force is exerted on the carriers of the semiconductor, pushing them to the ends and creating the V_H voltage. The potential difference occurs due to the perpendicularity of the magnetic field lines and the current flow, however, appropriate polarity is also required. Hall potential difference (Hall voltage) relies on the amount and directions of magnetic field and electric current (power supply). [10]

Each time the N or S pole of the magnet passes near a Hall sensor, the sensor generates a high or low signal respectively, indicating the polarity of the pole. The specific sequence of commutation can be calculated, depending on the combination of the three Hall sensor signals. [9]

Magnetic sensors are solid state devices that are becoming increasingly prevalent because they can be used in several application categories such as sensing location, velocity or directional movement. They are also a common sensor option for the electronics manufacturer because of their wear-free non-contact activity, low cost, durable construction and being resistant to vibration, dust and water as enclosed Hall Effect sensors. [10]

Hall effect sensors can have linear output or digital output. For linear output the output signal is taken directly from the output of the operational amplifier. The output voltage is proportional to the magnetic field passing through the Hall sensor. Linear sensors get a continuous voltage output which increases with a high magnetic field and decreases with a low magnetic field. Also, the output signal will increase as the strength of the magnetic field increases until the time it starts to saturate by the limitations set on it by the power supply, as shown in Figure 2.5. Any further magnetic field increase will have no impact on the output. [10]

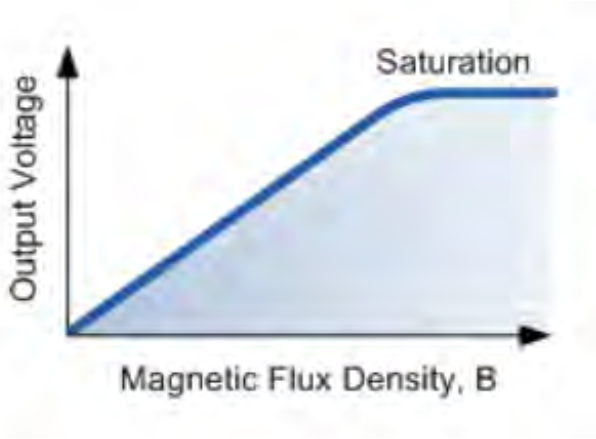

Figure 2.5 Representation of the output of the Hall sensor as a function of magnetic flux density

At the other side, digital output sensors have a Schmitt trigger with built in hysteresis, after the amplifier output, in order to convert the analog signal to digital. When the magnetic flux passing through the Hall sensor exceeds a predetermined value, its output goes from state "OFF" to "ON". The built-in hysteresis of the comparator avoids any oscillation of the output signal as the sensor is affected or not by the magnetic field during rotation of the rotor, resulting in only two output states. The following Figure 2.6 shows the sensor circuit. [11]

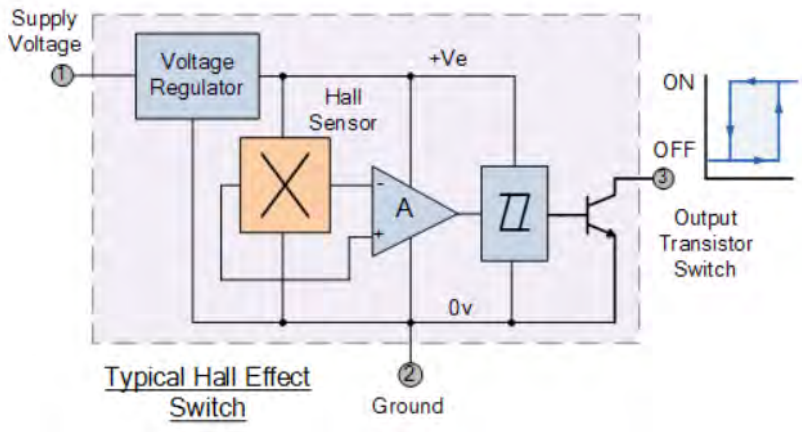

Figure 2.6 Hall sensor circuit with digital output

There are two basic types of Hall Effect digital sensor, Bipolar and Unipolar. Bipolar sensors are activated by a positive magnetic field (south pole) and deactivated by a negative field (north pole). Monopolar sensors require a magnetic south pole to activate them and deactivate them, as they are passing through a magnetic field or not, respectively. [11]

Finally, an NPN transistor is added to the output of the circuit for large current loads. This transistor operates in the saturation range, short-circuiting the output each time the load current exceeds the preset limit. [11]

2.2.1 Rotor

The rotor has cylindrical shape and on its surface are placed permanent magnets, the number of which varies from two to eight pairs of poles with opposite polarity. The pole number differs according to the application demands. Nevertheless, the number of poles is a counterbalance between torque and speed. This ensures that the greater pole number the better torque the rotor provides as it decreases the maximum achievable speed. [8]

Concerning the choice of magnetic material for the construction of the rotor is based on the required magnetic field density. Ferrite is a material that is, traditionally, used to make permanent magnets. However, as technology evolves, rare earth magnets are becoming more popular. Ferrite magnets are less costly but have the downside of low flow density for a fixed amount volume. In contrast, alloys have a high flow density per

volume and so the rotor volume can be reduced for the same torque. Alloys, also, improve the size-to-weight ratio, achieving greater torque for the same motor size than using ferrite magnets. The placement of the magnets on the rotor can be done in various ways, as shown in Figure 2.7. [7]

Figure 2.7 In the first rotor the magnets are placed on the surface of the rotor, in the second the magnets are embedded horizontally in the cursor, and in the third they are placed vertically

2.3 The operation principle of BLDC motor

BLDC motor is a kind of synchronous motor. That means that the stator electromagnetic field rotates at the same frequency is the rotor magnetic field. [12] The energized stator phase attracts the rotor magnets and forces the rotor to move. BLDC motor operation requires the rotor position information. Based on the rotor position, the phase windings are switched in a sequence to achieve its rotation. In many BLDC motor drives a current control loop is used to sustain the load current at some desired level. This is achieved by switching the constant DC link voltage across the motor windings. [13] Every commutation sequence has one of the windings connected to positive supply (current enters into the winding), the second winding is connected to negative supply (current exits the winding) and the third is in a non-energized condition. [9]

In order to carry on the rotation of the motor, the magnetic field produced by the windings should change position, as the rotor moves to meet up with the stator field. The sequence of energizing the windings is determined by a process which is called “Six-Step Commutation”. The six-step commutation energizes two motor phase windings at any commutation sequence. Every step is equivalent to 60 electrical degrees, so six steps

make a full 360° rotation. The current can be controlled by a full 360 degree loop, due to the fact that there is only one current path. [9]

Six-step commutation is efficient at managing motor speed, however, at low speed it struggles with torque ripple throughout commutation. Therefore, it is suitable in applications that involve high speed and commutation frequencies. Also, it is common in low-end applications that demand an easy closed-loop function. But in the commutation scheme there is a large torque ripple caused by the non-linearities, since only two windings carry current. The non-linearities cause noise and vibration. A six-step BLDC Motor usually has lower torque efficiency than a sine-wave commutated motor. [9] [5]

2.4 The control method of BLDC motor rotation

Hall sensors reserve to the motor the control of the rotor motion by accurately defining its position inside the stator. The sensors provide the appropriate sequence in order to activate the switches on the inverter bridge, the arrangement of which is illustrated in Figure 2.8. Depending on the rotor position, the switches are changed sequentially every 60 ° (electrical degrees). After the rotor position is detected, the appropriate phases are conducting through the electronic commutation. [14]

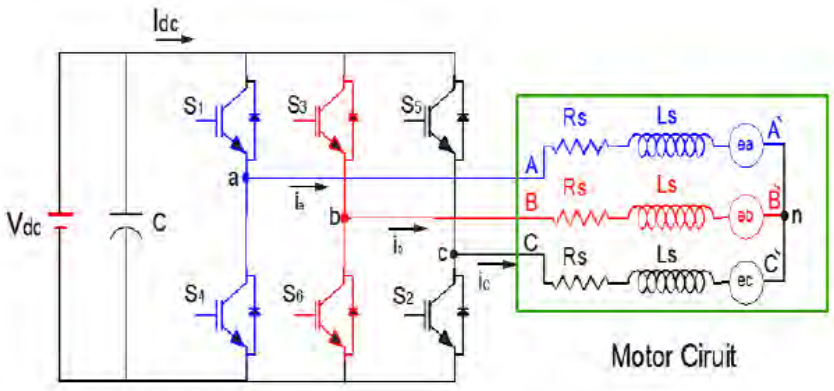

Figure 2.8 Motor connection to the inverter

Figure 2.8 shows a representation of the internal connection of the inverter to the motor, which consists of the three windings in the stator and the rotor on which the permanent magnet is placed (1 pole-pair - 1 pole pair). The permanent magnet creates a magnetic

field while the excited stator windings are converted into electromagnetic poles, creating an electromagnetic field. The coexistence of these two magnetic fields between rotor and stator, results in the development of torque which tends to align them. This torque causes the rotor motion trying to align its magnetic field with the stator magnetic field. At this point it is worth noting that the two magnetic fields are never fully aligned, as this would lead to zero torque and therefore immobilization of the rotor. This is achieved by timely change of the conducting phases.

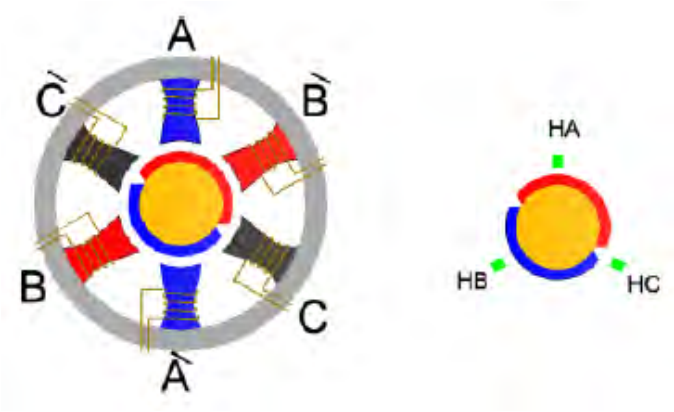

Figure 2.9 Structure of BLDC motor

The polarity reverse of the stator windings is achieved through the semiconductor power switches. The three sensors HA, HB and HC, which are arranged as shown in Figure 2.9, are responsible for generating the signals required to switch on the appropriate switches. Each time a Hall signal changes state, the conducting phases change.

In Table 2.4 is shown the switching sequence which is used for clockwise rotation of the motor. Every 60° of rotation, one of the three Hall sensors changes state, leading to another sequence. Six steps are required to complete an electrical cycle. [2]

At this example the number of electrical cycles happens to be the same as the number of mechanical cycles due to the 1 pole-pair used in the rotor. One electric cycle, however, may not correspond to a mechanical cycle. That is happening due to the fact that the number of electrical cycles is depending on the number of pole-pairs placed in the rotor. Therefore, the number of electrical cycles equals to the pole-pair number. [7]

Table 2.4 Sequence for rotating the motor in clockwise direction

Sequence	Hall sensor A (HA)	Hall sensor B (HB)	Hall sensor C (HC)	Active Switches	Phase Current A	Phase Current B	Phase Current C
1	1	1	0	S3,S2	0	+1	-1
2	1	0	0	S1,S2	+1	0	-1
3	1	0	1	S1,S6	+1	-1	0
4	0	0	1	S5,S6	0	-1	+1
5	0	1	1	S5,S4	-1	0	+1
6	0	1	0	S3,S4	-1	+1	0

Figure 2.10 shows the Hall sensor signals relative to the Back-EMF and phase currents.

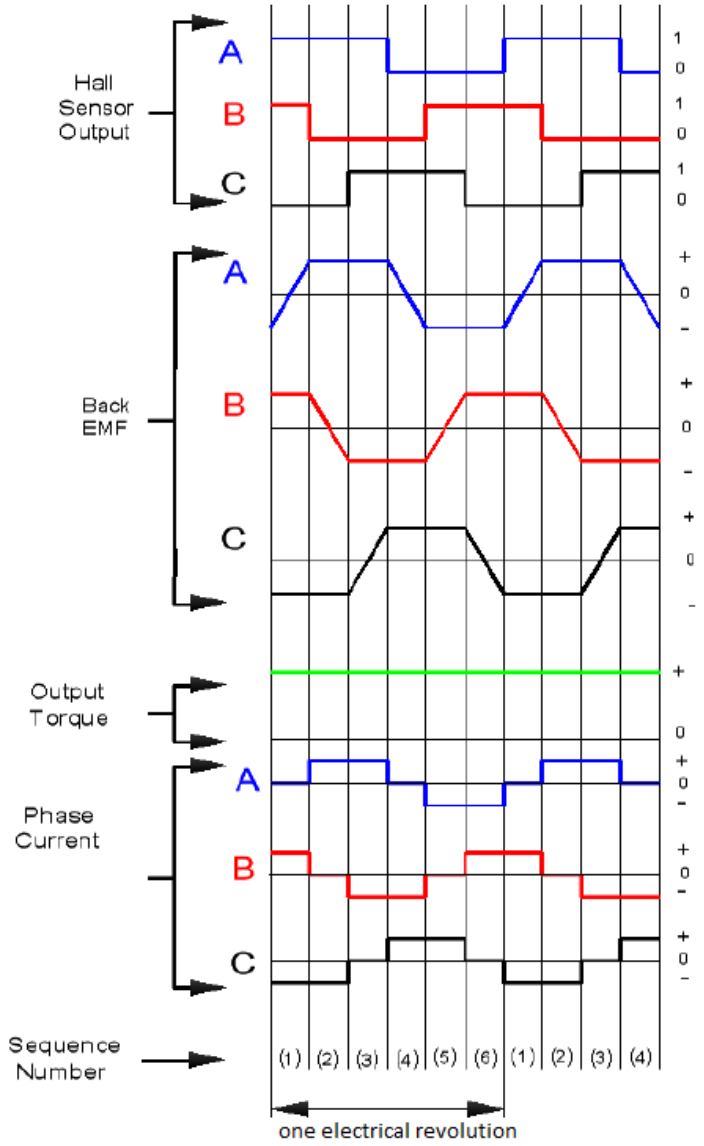

Figure 2.10 Wave forms of Hall sensors, BEMF, torque and phase currents

Subsequently, follows a representation of the magnetic forces exerted during the rotation of the rotor by 120°, based on the data in Table 2.4 and the graphs in Figure 2.10. Indicatively, for sequence 4 S_5 and S_6 are switched on, causing the current to enter from phase C and exit from phase B, while at the same time phase A is floating. In Figure 2.11 the conducting stator windings are shown and also the electromagnetic field (Φ_{ST}) that they cause, as well as the magnetic field of the rotor (Φ_R), which forms 120° with the electromagnetic field of the stator. [2]

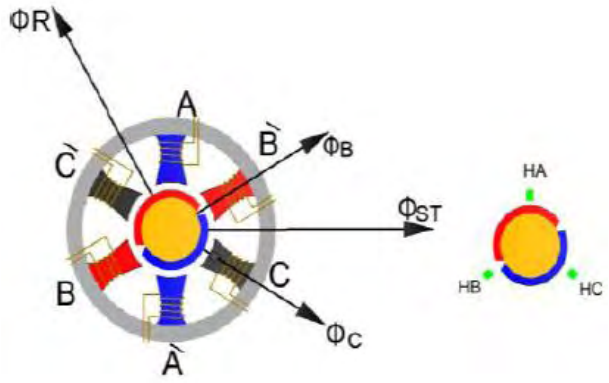

Figure 2.11 Representation of motor magnetic fields at sequence 4

Assuming, the magnetic fields of rotor and stator differ by 120° at the beginning of the commutation in this sequence, then after 30° the position of the rotor shifts as shown in Figure 2.12. [2] At this point the fields are 90° apart. It is worth mentioning that while these two fields are at 90° to each other the maximum torque occurs. [12]

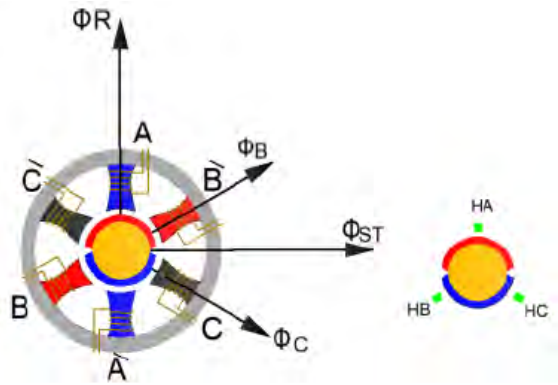

Figure 2.12 Representation of motor magnetic fields with 90° difference

By doing the same assumption at the end of sequence 4 and before the beginning of sequence 5, the stator magnetic field remains the same, while the rotor magnetic field has moved by a further 30° clockwise, as shown in Figure 2.13. The angle between the magnetic fields of the stator and the rotor is 60°. The relative position between the magnetic fields of the stator and the rotor ranges between 60° and 120° with an average value of 90°. [2]

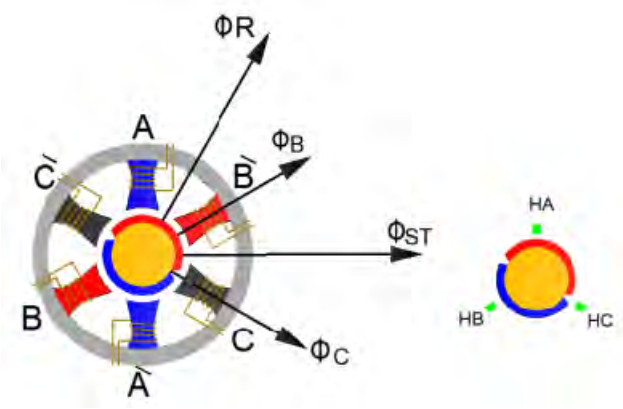

Figure 2.13 Representation of motor magnetic fields with 60° difference

2.5 Mathematical model of BLDC motor

Considering a three-phase BLDC motor in star connection, with the assumption that $R_a = R_b = R_c = R$ due to symmetry of three-phase BLDC motor and $L_a = L_b = L_c = L = L_s - M$, the equivalent circuit is arranged as shown in Figure 2.14. Here, the small letters a, b and c denote the phases of the BLDC motor. [8]

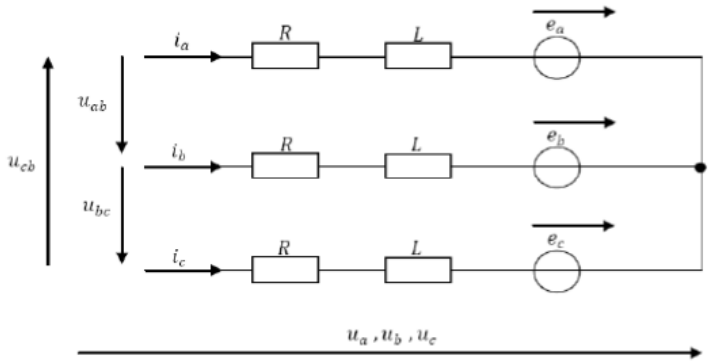

Figure 2.14 The equivalent circuit of three-phase motor star-connection

The following equations describe the equivalent circuit:

$$u_a = Ri_a + L\frac{di_a}{dt} + e_a \tag{2.1}$$

$$u_b = Ri_b + L\frac{di_b}{dt} + e_b \tag{2.2}$$

$$u_c = Ri_c + L\frac{di_c}{dt} + e_c \tag{2.3}$$

Thus,

$$u_{ab} = R(i_a - i_b) + L\frac{d}{dt}(i_a - i_b) + e_a - e_b \tag{2.4}$$

$$u_{bc} = R(i_b - i_c) + L\frac{d}{dt}(i_b - i_c) + e_b - e_c \tag{2.5}$$

$$u_{ca} = R(i_c - i_a) + L\frac{d}{dt}(i_c - i_a) + e_c - e_a \tag{2.6}$$

Where,

R: Armature resistance

L_s: Armature inductance

M: Mutual inductance, which describes the flux linkage between two windings

$e_{a,b,c}$: The Back-EMF

$i_{a,b,c}$: The armature currents flowing through windings

$u_{a,b,c}$: The phase voltages

u_{ab}, u_{bc}, u_{ca}: The phase-to-phase voltages

The phase currents are associated with the Equation (2.7):

$$i_a + i_b + i_c = 0 \tag{2.7}$$

Since each voltage is a linear combination of the other two voltages, the system can be described by using two equations. By removing one equation and eliminating one variable using Equation (2.7), Equation (2.4) and Equation (2.5) can be written as:

$$u_{ab} = R(i_a - i_b) + L\frac{d}{dt}(i_a - i_b) + e_a - e_b \tag{2.8}$$

$$u_{bc} = R(i_a + 2i_b) + L\frac{d}{dt}(i_a + 2i_b) + e_b - e_c \tag{2.9}$$

From the Newton's second law of motion, the relation between electromagnetic torque T_e and speed of motor ω_m can be written as following:

$$T_e - T_l = J\frac{d\omega_m}{dt} + B\omega_m \tag{2.10}$$

$$\omega_m = \frac{d\theta_m}{dt} \tag{2.11}$$

Where,

T_l: Load torque in Nm

J: Moment of inertia in kg/m^2

B: Damping constant

The Back-EMF and electromagnetic torque can be expressed as:

$$e_a = \frac{k_e}{2}\omega_m F(\theta_e) \tag{2.12}$$

$$e_b = \frac{k_e}{2}\omega_m F\left(\theta_e - \frac{2\pi}{3}\right) \tag{2.13}$$

$$e_c = \frac{k_e}{2}\omega_m F\left(\theta_e - \frac{4\pi}{3}\right) \tag{2.14}$$

$$T_a = \frac{k_t}{2} i_a F(\theta_e) \tag{2.15}$$

$$T_b = \frac{k_t}{2} i_b F\left(\theta_e - \frac{2\pi}{3}\right) \tag{2.16}$$

$$T_c = \frac{k_t}{2} i_c F\left(\theta_e - \frac{4\pi}{3}\right) \tag{2.17}$$

Thus

$$T_e = \frac{k_t}{2}\left[F(\theta_e) i_a + F\left(\theta_e - \frac{2\pi}{3}\right) i_b + F\left(\theta_e - \frac{4\pi}{3}\right) i_c\right] \tag{2.18}$$

Where k_e and k_t are Back-EMF constant and electromagnetic torque constant respectively. The electrical angle θ_e is equal to the mechanical angle θ_m of motor multiplied by the number of pole pairs ($\theta_e = \frac{p}{2}\theta_m$). The function $F(\theta)$ is a function of rotor position, which gives the trapezoidal waveform of Back-EMF. One period of function can be given as:

$$F(\theta_e) = \begin{cases} 1, & 0 \le \theta_e < \frac{2\pi}{3} \\ 1 - \frac{6}{\pi}\left(\theta_e - \frac{2\pi}{3}\right), & \frac{2\pi}{3} \le \theta_e < \pi \\ -1, & \pi \le \theta_e < \frac{5\pi}{3} \\ 1 + \frac{6}{\pi}\left(\theta_e - \frac{2\pi}{3}\right), & \frac{5\pi}{3} \le \theta_e < 2\pi \end{cases} \quad (2.19)$$

Due to the symmetry design of motor, the Back-EMF signal of each phase is 120 degrees phase shifted with respect to each other as shown in Figure (2.15)

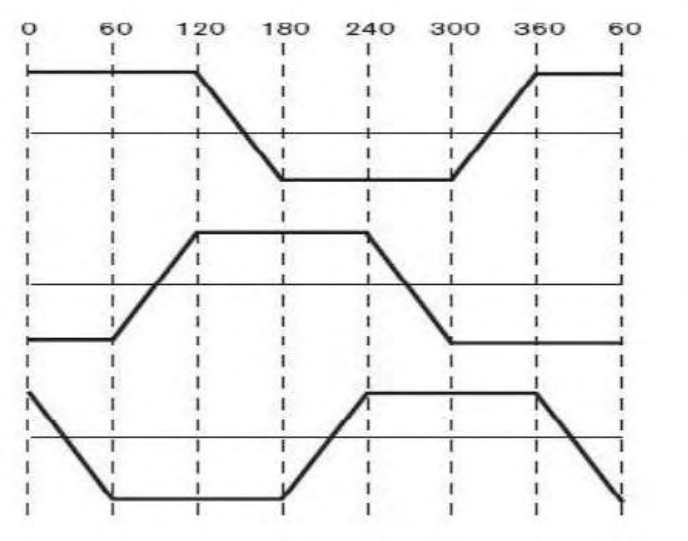

Figure 2.15 Back-EMF signals with 120 degrees phase shift

2.6 Sensorless operation of BLDC motor

There are some drawbacks to the use of position sensors. The sensors increase the complexity of the motor, not only because of the motor construction complexity, but also because they require great precision in their placement. Any mistaken position of the sensors could reduce their reliability. Also, they increase the cost and the size of the motor and they present sensitivity in high temperatures. As a consequence, the use of sensorless methods is an alternative way for determining commutation on a BLDC motor. Some of the methods, that are developed to detect the rotor position, are described in this section.

2.6.1 Back-EMF Zero Crossing Point Detection method

The BLDC motor consists of three stator windings connected to the neutral point (n), as shown in Figure 2.16 which represents the motor connection to the three-phase inverter.

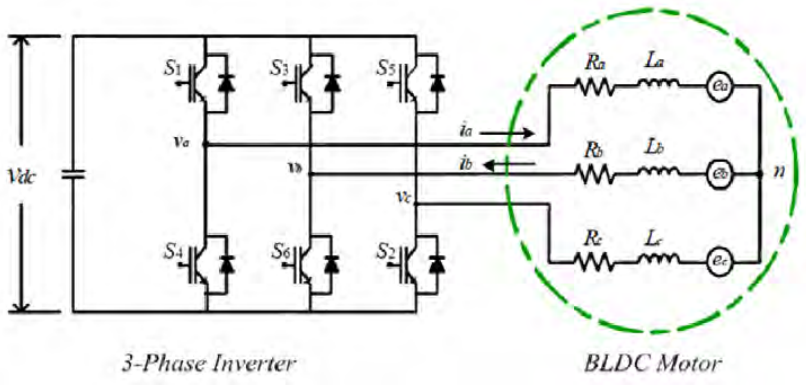

Figure 2.16 BLDC motor and inverter block diagram

The voltage equation of the motor, concluding the neutral point, cam be expressed as:

$$\begin{bmatrix} V_a \\ V_b \\ V_c \end{bmatrix} = R \begin{bmatrix} i_a \\ i_b \\ i_c \end{bmatrix} + L \frac{d}{dt} \begin{bmatrix} i_a \\ i_b \\ i_c \end{bmatrix} + \begin{bmatrix} e_a \\ e_b \\ e_c \end{bmatrix} + \begin{bmatrix} V_n \\ V_n \\ V_n \end{bmatrix} \quad (2.20)$$

Where,

V_x, the terminal voltage

i_x, the phase current

e_x, the Back-EMF

Where *x* = *a*,*b*,*c*

R, the stator resistance

L, *the* stator inductance

V_n, the neutral voltage

The ZCP (Zero Crossing Point) detection of the BEMF waveform of floating phase is the basis of numerous sensorless methods. Figure 2.17 shows how the current is related to

BEMF, including the zero crossing points and the commutation instants. It is observed that commutation instants are lagged 30° behind the zero crossing points.

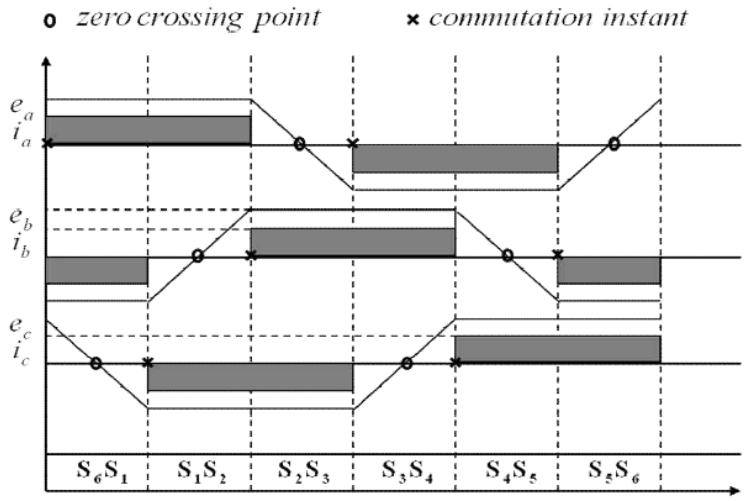

Figure 2.17 BEMF and current of each phase

It is obvious that ZCP detection requires the phase BEMF. However, for calculating the phase voltages it is needed the neutral point that is not included in the construction of a motor. The detection of ZCP is achieved by using the terminal voltage. As it is shown in Figure 2.18, the half of terminal voltage is synchronized with the ZCP of BEMF. [15]

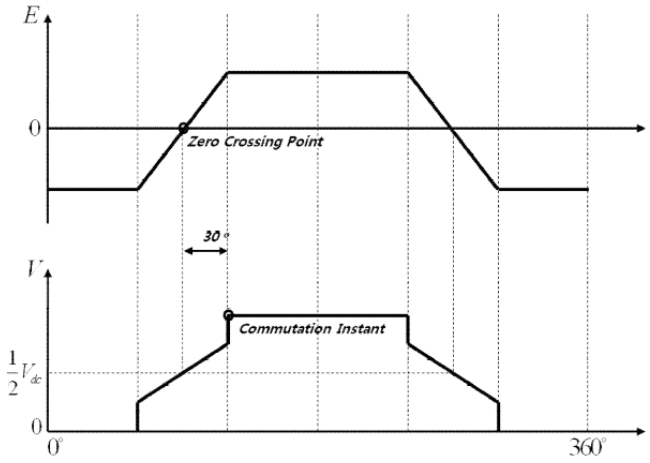

Figure 2.18 BEMF and terminal voltage

After ZCP detection, a timer is activated specifying the time for the next commutation instant. The timer is implemented by RC circuits. Figure 2.19 and Figure 2.20 represent

two different circuits composed of resistances, low pass filters and comparators. In Figure 2.19 the comparator uses as an input the half of the link DC voltage, unlike Figure 2.20 where comparator uses the neutral voltage. [15]

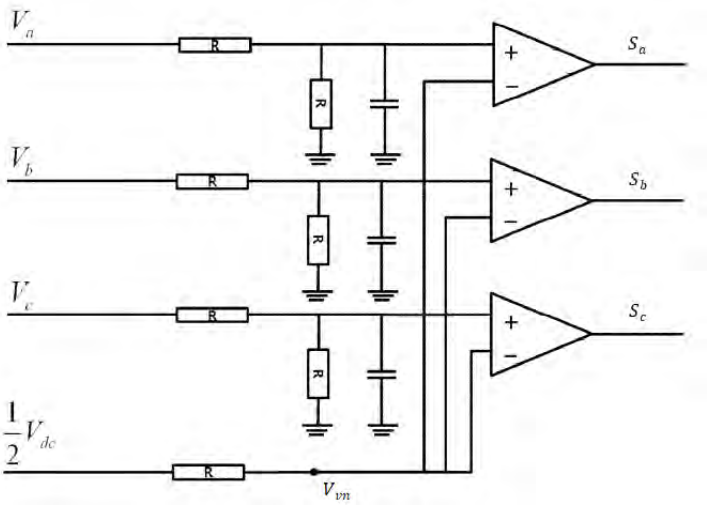

Figure 2.19 Half of DC link voltage based circuit

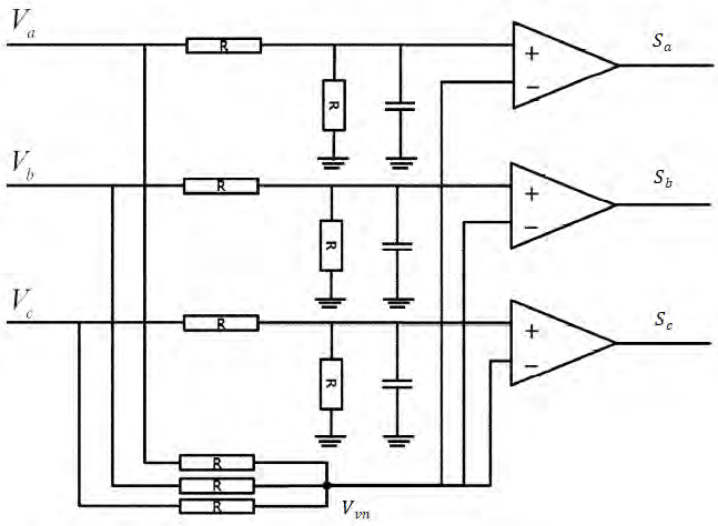

Figure 2.20 Virtual neutral voltage based circuit

Considering that phase A and phase B are energized an phase C is floating, the currents and the neutral voltage can be expressed as:

$$i_a = -i_b \,,\; i_c = 0 \tag{2.21}$$

$$V_n = \frac{1}{2}(V_a + V_b) \tag{2.22}$$

As it shown in Equation (2.22), the neutral voltage is equivalent to the half of link DC voltage, provided that the stator resistances are small and the neutral point can be manufactured by parallel resistance network with high value. [15]

$$V_n = \frac{1}{2} \cdot V_{dc} \approx V_{vn} \tag{2.23}$$

From Equation (2.21) and Equation (2.22), the terminal voltage of floating phase can be expressed as:

$$V_c = e_c + \frac{1}{2} \cdot V_{dc} \approx e_c + V_{vn} \tag{2.24}$$

Similarly,

$$V_a = e_a + \frac{1}{2} \cdot V_{dc} \approx e_a + V_{vn} \tag{2.25}$$

$$V_b = e_b + \frac{1}{2} \cdot V_{dc} \approx e_b + V_{vn} \tag{2.26}$$

Consequently, the terminal voltage of the floating phase is related to BEMF and the ZCP detection can be achieved by detecting the half of link DC voltage. Therefore, both circuits output signals which are equivalent to Hall sensor signals

PWM inserts harmonic components to the terminal voltage, causing noise. The use of first-order low pass filter is required to reduce the noise. The phase response of the first-order low pass filter can be expressed as: [15]

$$\theta = \tan^{-1}\left(\frac{R_a \cdot R_b}{R_a + R_b}\right) \cdot C \cdot \omega \tag{2.27}$$

where,

θ, the phase delay

R_a και R_b, are divider resistors

C, is the filter capacitor

ω, is the angular frequency related with the duty cycle of PWM

From Equation (2.27), the phase difference between the ZCP and the commutation instant can be expressed as:

$$\varphi = 30° - \theta \tag{2.28}$$

Where,

φ, the phase difference

Despite the fact that the filter lags 30° behind the ZCP of BEMF, the phase delay changes for different rotor speed values. As an effect, the phase recovery is complicated and the torque ripple increases because of inaccurate commutation.[15]

An additional issue with this method is that it requires a boot process. This is because BEMF cannot be detected when the motor is stationary or rotates at a low speed, and ZCP can be detected when the floating phase voltage exceeds the half of the link voltage. As a result, the motor functional range is restricted. [15]

2.6.2 BEMF difference method

This method uses the BEMF difference to determine the commutation instants. As shown in Figure 2.21, the ZCP of BEMF difference corresponds to the commutation instant.

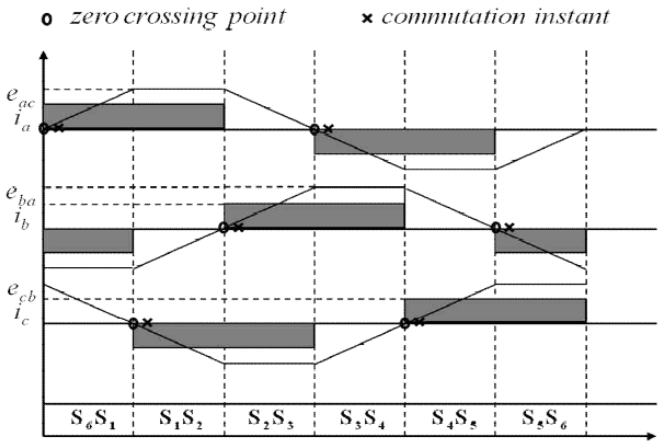

Figure 2.21 BEMF difference and current of each phase

As BEMF difference cannot be used, the detection of ZCP is achieved by using the terminal voltage difference. As shown in Figure 2.22, the ZCP of BEMF difference is synchronized with the ZCP of terminal voltage difference. Therefore, ZCP of terminal voltage difference can be used for determining commutation instant without applying phase delay. [15]

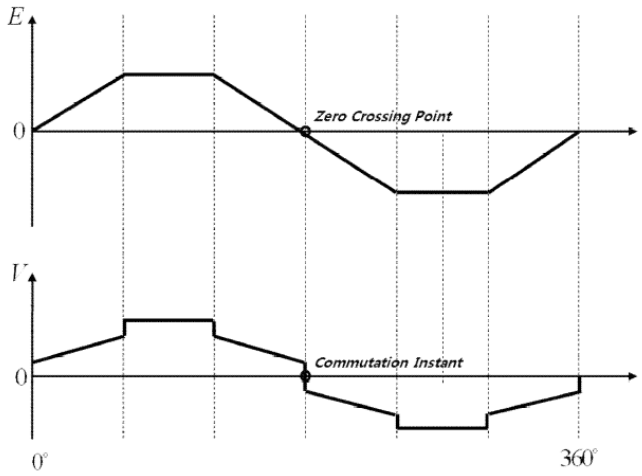

Figure 2.22 BEMF difference and terminal voltage

From Equation (2.20), the voltage difference between terminal A and terminal C can be expressed as:

$$V_{ac} = R \cdot (i_a - i_c) + L\frac{d}{dt}(i_a - i_c) + (e_a - e_c) + (v_n - v_n)$$

$$= R \cdot i_{ac} + L \cdot \frac{d}{dt} \cdot i_{ac} + e_{ac} \quad (2.29)$$

Similarly,

$$V_{ba} = R \cdot i_{ba} + L \cdot \frac{d}{dt} \cdot i_{ba} + e_{ba} \tag{2.30}$$

$$V_{cb} = R \cdot i_{cb} + L \cdot \frac{d}{dt} \cdot i_{cb} + e_{cb} \tag{2.31}$$

Where,

V_x, the voltage difference

i_x, the current difference

e_x, the BEMF difference

Where, x = ac, ba, cb

Assuming that phase A or phase C is floating, voltage difference V_{ac} depends on the BEMF alteration of every phase. It is worth noting that the period during which phase A is floating precedes the period during which phase C is floating, and the ZCP detection of the BEMF difference is placed exactly in the middle of these two periods. The terminal voltage difference can be expressed as: [15]

$$V_{ac} = \begin{cases} -R \cdot i + e_{ac} & (A\ is\ floating) \\ R \cdot i + e_{ac} & (C\ is\ floating) \end{cases} \tag{2.32}$$

It results from Equation (2.32) that the ZCP of BEMF difference can be extract comparing the terminal voltage difference with the power ground of link DC voltage, generating the commutation signal for phase A. By implementing the same process for terminal voltage differences V_{ba} and V_{cb} , the commutation signals for phase B and C will be generated. Figure 2.23 illustrates the circuit which is configured to generate the commutation signals. It is composed of two amplifier stages. [15]

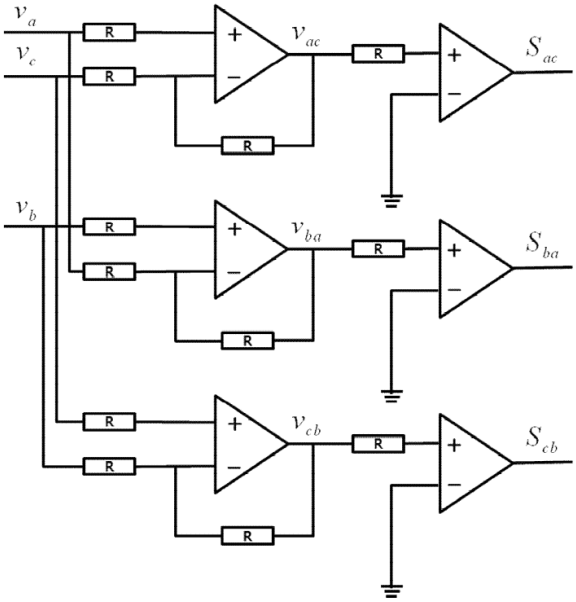

Figure 2.23 BEMF difference method circuit

In the first stage the circuit outputs the terminal voltage difference and in the second stage it compares the terminal voltage difference with the power ground. After this process the commutation signal is generated, replacing a sensor signal. In the case of using this circuit a boot process is not needed, as the BEMF can be detected just when the rotor starts moving. [15]

2.6.3 Back-EMF integration method

In this method, the phase commutation is specified by integrating the BEMF of floating phase. As it shown in Figure 2.24, the integration area is similar at different rate of speeds. The integration period starts from the ZCP of BEMF until the integrated value reaches a threshold value, which gives the corresponding commutation instant and the phase gets commutated. [16]

The integration approach decreases the switching noise sensitivity and it is easy adjustable to speed alterations. However, this method is not effective in low motor speeds because of the errors and offset voltage problems caused by integration. Since BEMF is altered linearly from positive to negative, due to its trapezoidal shape, without displaying any speed sensitivity, the threshold is stable in each speed rate. [16]

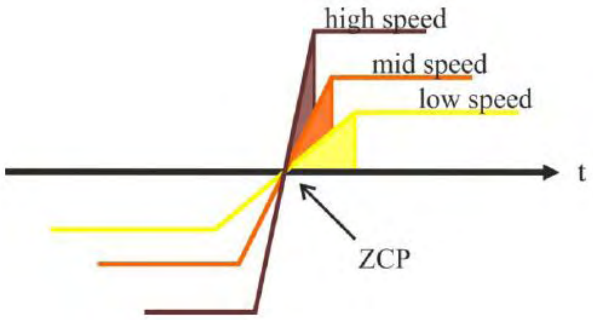

Figure 2.24 Integrated areas of the back-EMF

A reset signal is declared to zero the integrator output until the integrated value reaches the threshold voltage. The reset signal maintains its condition stable until the BEMF waveform of floating phase crosses zero. [16]

BEMF integration method is improved related to the ZCP detection method, in which the zero crossing point detection of BEMF leads to activation of a timer. Here the BEMF is given as an input to an integrator and the output value compares to a threshold value. This method presents several drawbacks of decreased switching noise sensitivity and it is adjustable to speed alterations.[16]

2.6.4 Free-wheeling diodes conduction detection method

In this method the rotor position detection is achieved by inspecting the conducting state of antiparallel connected free-wheeling diodes in the floating phase. Knowing the free-wheeling diode conducting state, the ZCP of BEMF can be extracted. [17]

As the current of the floating phase arises from BEMF, the rotor position cannot be determined while motor is stationary. Thus, a boot process is needed to generate a commutation signal for starting the rotor movement. The implementation of this process includes the conduction of two arbitrary phases for a predetermined time. The rotor moves based on the conducted phases. At the end of predetermined time, the phase commutation sequence is followed by 120° and the polarity of the currents is changed. [16]

This method has an advantage over previous BEMF detection methods, as it makes it possible to detect the rotor position at a wide range of speeds and especially at lower speeds. However, one disadvantage is the use of six separated power supplies for the

comparator circuit to detect the current flowing through each diode. [16] [17]

2.5.5 Third Harmonic Voltage Integration method

In this method commutation instants results from the third harmonic of the BEMF waveform. Fundamental and other polyphase components are excluded by the summation of the three terminal voltages, as shown in Equation (2.33). [16]

$$V_{SUM} = V_{AN} + V_{BN} + V_{CN} \approx (e_A + e_B + e_C) \approx 3 \cdot E_3 \cdot \sin(3 \cdot \omega_e \cdot t) \qquad (2.33)$$

By integrating the third harmonic voltage component to estimate the rotor flux linkage as shown in Equation (2.34), the zero crossing point of waveform, and thus, the commutation instants can be detected.

$$\lambda_{r3} = \int V_{SUM} \cdot dt \qquad (2.34)$$

Moreover, there is a limited filter demand, as the frequency of the third harmonic signal is three times greater than the simple signal and it can be detected at low speeds, enabling the motor to operate in many different speed levels. Also, advantages of this method are the simplicity of its application, the precise synchronization of the ZCP with the phase commutation instants and the low sensitivity to the electric noise. [17]

Figure 2.25 shows the BEMF of phase A, the third harmonic signal V_{SUM}, the rotor flux third harmonic component λ_{r3}, the rotor flux λ_r and the stator phase currents. It is noticed that the commutation instants correspond to ZCP of the third harmonic component.

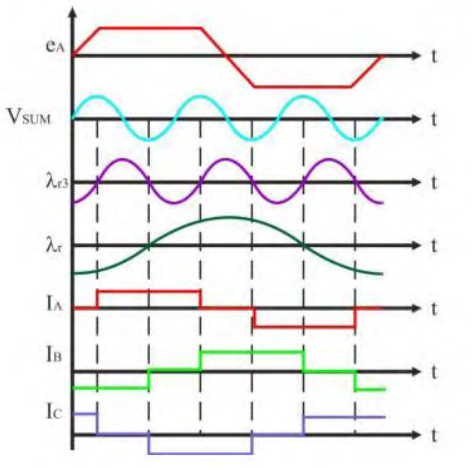

Figure 2.25 BEMF, third harmonic voltage, rotor flux fundamental components, rotor flux and motor phase currents

CHAPTER 3

CONTROL SYSTEM OF BLDC MOTOR

3.1 Closed loop control of BLDC motor

The operation of a BLDC motor is achieves through a closed loop control. The inner loop synchronizes the pulses of the inverter bridge with the BEMF and the outer loop controls the speed. In Figure 3.1 is shown the block diagram of speed control.

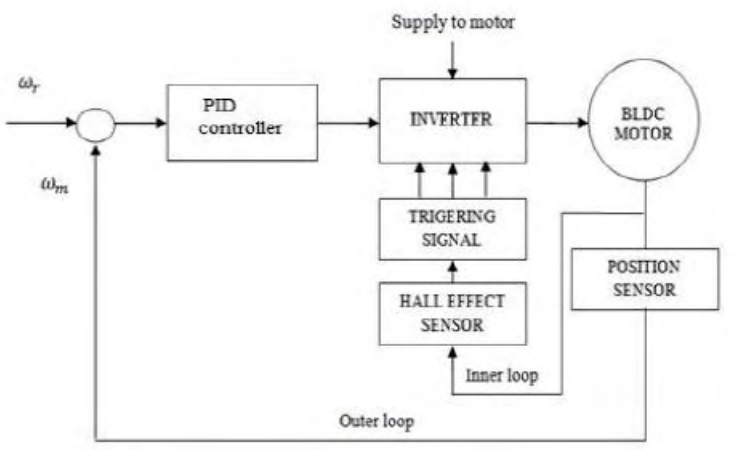

Figure 3.1 Closed loop speed control of BLDC motor

A conventional BLDC motor drive is generally implemented through a six-switch three phase inverter and three Hall effect position sensors that provide six commutation points for each electrical cycle. The sensors provide the correct switching sequence for turning on the appropriate switches in the inverter bridge. This information comes from the rotor position feedback. The inverter is responsible for converting the power from the source to generate the motor, which then transforms the receiving voltage to mechanical torque of the rotor. [14]

Because of nonlinearity of current winding with rotor speed, it is important to have an accurate speed control. Rapid recovery of the reference speed is necessary for in time speed alteration. The PID controller is suitable for these control issues, as it is very sensitive to the gradual speed alterations, changes of parameters and load disturbances. [1]

The difference between the measured and required speeds is inserted to the PID controller. According to this data controller configures the duty cycle of the PWM pulses which is related to the voltage amplitude which is demanded sustain the desired speed. By using the PWM signal as an input to the switches of the inverter, modification of the motor voltage can be managed easily by adjusting the duty cycle of PWM. [1]

3.1.1 Back Electromotive Force (BEMF)

During the rotation of the motor, the windings generate a voltage named Back Electromotive Force (BEMF). Due to Lenz's law this voltage opposes the supplied voltage to the windings. BEMF is affected by the angular velocity developed in the rotor, the rotor magnetic field and also the number of turns in the stator windings (as shown in equation 3.1). However, because of the fact that the magnetic field and the number of turns in the windings are stable, the BEMF is affected only from the rotor speed. The increase of the speed leads to increase of BEMF. [7]

$$Back\ EMF = (E) \propto NlrB\omega \tag{3.1}$$

Where,

N , the number of winding turns per phase

l , the length of the rotor

r, the internal radius of the rotor

B, the rotor magnetic field density

ω, the motor's angular velocity

Also, by using the technical electrical parameter Back EMF constant K_E $(V/rpm\ or\ V/rad/s)$, BEMF can be estimated for a given speed. Based on the BEMF constant which is given during the construction of the motor, it can operate in rated parameters. If the rotor moves at the rated speed then the motor is able to achieve the rated torque and the rated current in the stator windings. When the rotor moves above the rated speed, the windings' potential difference needs to be increased. The potential

difference is defined as the subtraction of the BEMF from the supply voltage. Therefore, the decrease of the BEMF leads to both a reduction in the potential difference and current. [7]

3.2 Three phase inverter

The drive of a BLDC motor is achieved through the three-phase voltage inverter. The conversion of direct voltage to alternating voltage, with variable frequency and amplitude, is managed with the use of electronic power converters. Figure 3.2 shows the equivalent circuit of a BLDC motor with three-phase inverter.

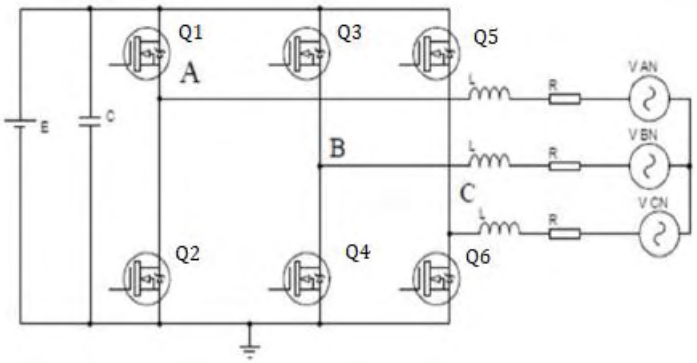

Figure 3.2 Three phase inverter based BLDC motor drive

As shown in Figure 3.2, L corresponds to the motor inductance and R corresponds to the resistance. V_{AN}, V_{BN} και V_{CN} are the BEMF of the motor. E corresponds to the battery and C is the capacitor at the entry of the inverter. While the specific inverter is a three-phase power semiconductor bridge, it consists of six semiconductor switches Q1 to Q6. [18]

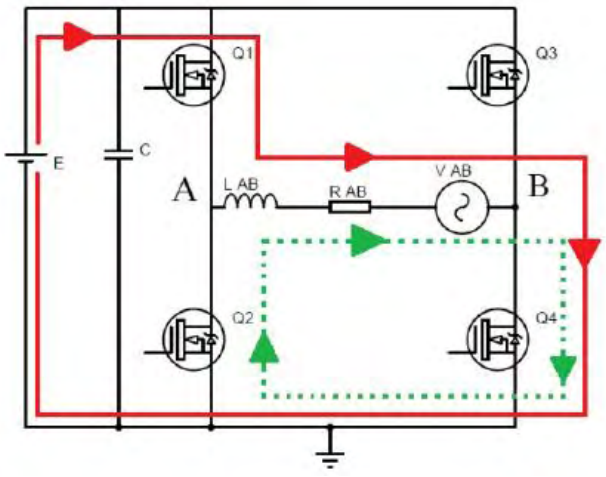

Figure 3.3 The inverter operation

In Figure 3.3 is shown a simulation of the inverter operation. Assuming that elements Q1 and Q4 conduct, which corresponds to a current flow from phase A to phase B (red line). After the phase commutation, the inductor holds energy and in the next commutation step the Q1 is switched off while the Q4 keeps being switched on. The inductor frees its energy through Q4 and the diode of Q2 (dashed green line). This operation is described for one commutation step that lasts 60 electrical degrees. In total, there will be six states corresponding to the six step commutation process, completing an electrical cycle (360°).

3.2.1 Power semiconductor switches

Diode

The diode is the simplest semiconductor power switch. It is responsible for controlling the flow of charge carries. The diode has two terminals, anode and cathode, as shown in Figure 3.4. It allows current to flow in one direction and blocks the flow to the opposite direction. [19]

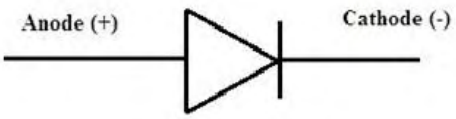

Figure 3.4 Diode

BJT (Bipolar Junction Transistor)

Transistors have three terminals (Emitter, Base, Collector) made from different semiconductor materials that can act as either an insulator or a conductor by applying a small signal voltage. They are separated in NPN and PNP transistors, as shown in Figure 3.5. NPN transistor is switched on when enough current is supplied from the transistor base to the emitter. This happens when Base is connected to a positive voltage and Emitter is connected to a negative voltage. When the amount of current is high enough, it starts to flow from the Collector to the Emitter. In PNP transistor, current flows from the Emitter to the Base, and then when the amount of current is high enough, it flows from the Emitter to Collector. [20]

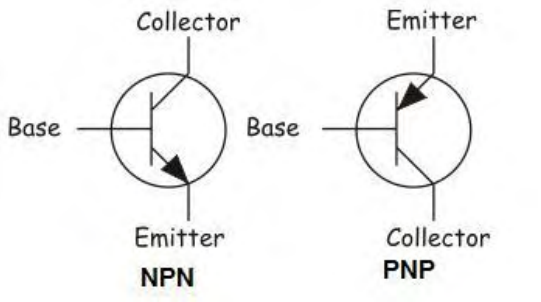

Figure 3.5 Bipolar Junction Transistor

MOSFET (Metal Oxide Semiconductor Field Effect Transistor)

MOSFETs are the most widely used field effect transistors in power switches. They have three terminals (Gate, Source, Drain) and they are separated in N-channel and the P-channel MOSFETs, as shown in Figure 3.6, depending on the existent channel between Drain and Source. MOSFETs are converted to N-channel when the applied gate voltage is negative and P-channel when the applied gate voltage is positive. MOSFET is a voltage controlled field effect transistor that has a "Metal Oxide" Gate electrode which is electrically insulated from the main semiconductor N-channel or P-channel by a very thin layer of insulating material usually silicon dioxide, commonly known as glass. [20]

As the Gate terminal is electrically isolated from the main current carrying channel between the drain and source, the current does not flow into the Gate. Also, the current flowing through the main channel between the Drain and Source is related to the input voltage. MOSFETs' operation is based on two different modes:

- *Depletion mode* : The transistor requires the Gate-Source voltage (V_{GS}) to switch off the device. For the n-channel depletion mode MOSFET, a negative gate-source voltage, -V_{GS}, will turn the transistor "OFF". Similarly, for a p-channel depletion mode MOSFET, a positive gate-source voltage, +V_{GS}, will turn the transistor "OFF". *T*he channel conducts when $V_{GS} = 0$. The depletion-mode MOSFET is less popular than the enhancement-mode type.
- *Enhancement mode* : The transistor requires the Gate-Source voltage (V_{GS}) to switch on the device. The Enhancement-mode MOSFET or eMOSFET, is the reverse of the depletion-mode type. The channel conducts when $V_{GS} = 0$. For an n-channel enhancement mode MOSFET, a positive gate-source voltage, $+V_{GS}$, will

turn the transistor “ON”, while a zero or -V_{GS} will turn the transistor “OFF”. For a p-channel enhancement mode MOSFET, a positive gate-source voltage, $+V_{GS}$, will turn the transistor “OFF”, while a zero or -V_{GS} will turn the transistor “ON”.

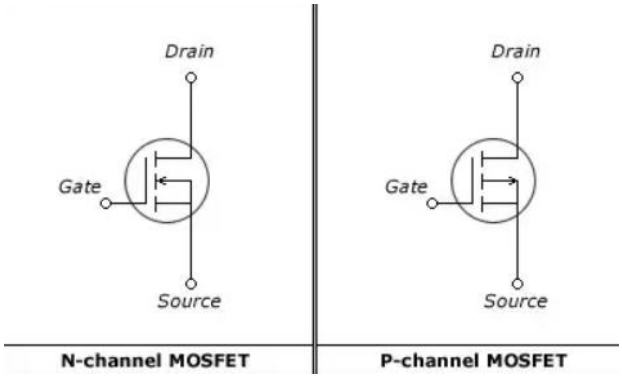

Figure 3.6 MOSFETs

IGBT (Insulated Gate Bipolar Transistor)

The IGBT is a combination of MOSFET and BJT. As shown in Figure 3.7, it has three terminals (Gate, Collector, Emitter). It combines the insulated gate technology of the MOSFET with the output performance characteristics of a bipolar transistor. IGBT behaves in the same way as the BJT, except that it is controlled by the voltage which is applied to the Gate, rather than the current which is applied to BJT’s Base. However, it is voltage-controlled like a MOSFET. [19]

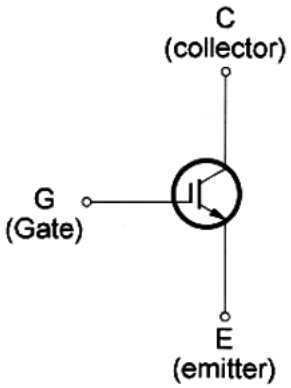

Figure 3.7 Insulated Gate Bipolar Transistor

3.3 Pulse Width Modulation control (PWM)

Pulse Width Modulation is a method during which the output of the inverter is regulated by modulating the input of the semiconductor switches. PWM is the procedure in which the reference waveform interacts with the carrier waveform in order to produce the triggering pulses to the switches. In Figure 3.8 is shown the block diagram for PWM inverter control of BLDC motor. After receiving the signals of the Hall sensors, the switching logic controller follows (switching logic) through which the appropriate switches of the inverter are activated. The desired speed is compared to the reference speed producing an error signal, which is then inserted to the PID controller. The control signal will modify the speed accordingly. [1]

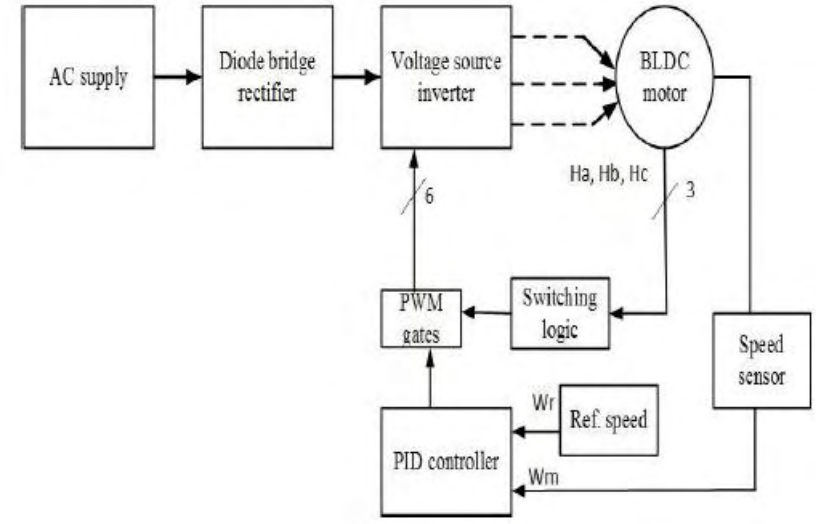

Figure 3.8 Block diagram for PWM inverter control of BLDC motor

As mentioned above the pulsation of the inverter is achieved by the pulse amplitude modulation method. The signals are created by comparing a rectangular reference signal of the amplitude, symbolized by A_r, with triangular carrier wave of amplitude, symbolized by A_c. The frequency of the output voltage is influenced by the frequency of the carrier wave. By changing the amplitude A_r from 0 to A_c, the pulse width can be varied from 0 to 100%. The ratio of A_r to A_c is the control variable and is known as the modulation index. The number of pulses per half cycle depends on carrier frequency. In Figure 3.9 is shown a simulink model of PWM technique for the creation of the pulses. [1]

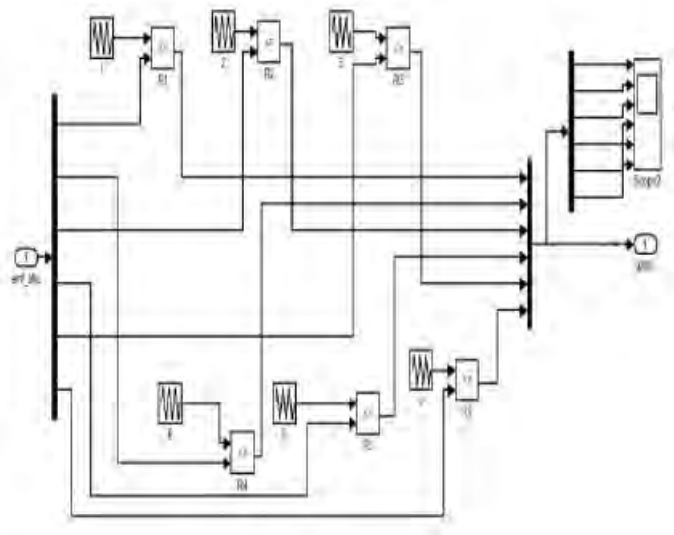

Figure 3.9 Simulink Model of Pulse Width Modulation Technique

3.4 PID controller (Proportional Integral Derivative)

The regulation of speed in a closed loop speed controlled is achieved by using a PID controller. PID controller is commonly applied in many procedures because it ensures decent performance by using a not complicated algorithm. The PID controller is implemented through different combinations of three types of controllers, which are distinguished in Proportional (P), Integral (I) and Derivative (D) controller. [21]

By using the suitable combination of the three components, the closed loop control can have the optimal output for different procedures. In a proportional controller the term K_p is proportional to the error. In integral controllers the term K_i/s is integral to the error. In derivative controller the term $K_d s$ is derivative to the error. PD controllers improve system's transient response while PI controllers reduce the steady state error present. PID controller provides both PD and PI controller's operations. [22]

PID controller minimizes the speed error and adjusts the PWM duty cycle. The error difference between the measured speed and reference speed is calculated at every PWM cycle and is given as an input to the controller. The feedback system of a PID controller is shown in Figure 3.10.

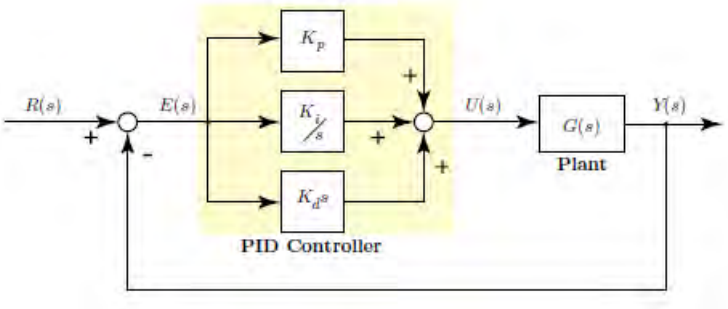

Figure 3.10 PID Controlled System

The controller calculates the error $e(t)$ between the reference value $r(t)$ and the measured value $y(t)$. The control signal $u(t)$ is the sum of three terms and every term is a function of the error $e(t)$. The controller function as a function of time is given as shown in Equation (3.2). [23]

$$u(t) = K_p e(t) + K_i \int_0^t e(\tau)d\tau + K_d \frac{de(t)}{dt} \tag{3.2}$$

The transfer function is defined as follows:

$$G_c(s) = K_p + \frac{K_i}{s} + K_d s \tag{3.3}$$

Where K_p, K_i, K_d are the gains of each term.

3.4.1 Interpretation of PID controller's terms

Considering that $K_i = K_d = 0$, the control signal $u(t)$ is given as shown in Equation (3.4). The control signal is proportional to the error signal. As a result, the bigger the difference between reference and measured speed is the most effort is required to achieve the desired speed. While the difference between reference and measured speed is getting smallest, the control is taken on the Integral term. [23]

$$u(t) = K_p e(t) \tag{3.4}$$

Considering that $K_p = K_d = 0$, the control signal is given as shown in Equation (3.5).

$$u(t) = K_i \int_0^t e(\tau)\, d\tau \tag{3.5}$$

If the system is unchangeable, it means that it has zero steady state. If error differs from zero while time passes, the control signal will be increasing. The Integral term can be assumed as the function of the past error values. The relation between the integral gain

and proportional gain is shown in Equation (3.6).

$$K_i = \frac{K_p}{\tau_i} \tag{3.6}$$

Where τ_i is the integral time. The Integral term is used to achieve the deceleration of the system response. In order to achieve the acceleration of the system response the Derivative term is used.

Considering that $K_p = K_i = 0$, the control signal is given as shown in Equation (3.7).

$$u(t) = K_p \frac{de(t)}{dt} \tag{3.7}$$

Derivative term depends on the rate of change of the error. The control signal is related to the rate of change of the error. This changing shows the progress of the error. Therefore, the derivative term can be assumed as a function of the future error values.

CHAPTER 4

MODELING OF BLDC MOTOR DRIVE SYSTEM

4.1 Simulation model

The modeling of BLDC motor's drive system is implemented in Simulink / Matlab environment. The overall system consists of smaller subsystems connected together to make the entire system functional. The main subsystems are the BLDC motor, the 3-phase inverter, the PI controller and the subsystem which is responsible for decoding the hall sensor signals and generating the commutation sequences. Figure 4.1 shows the complete simulation model.

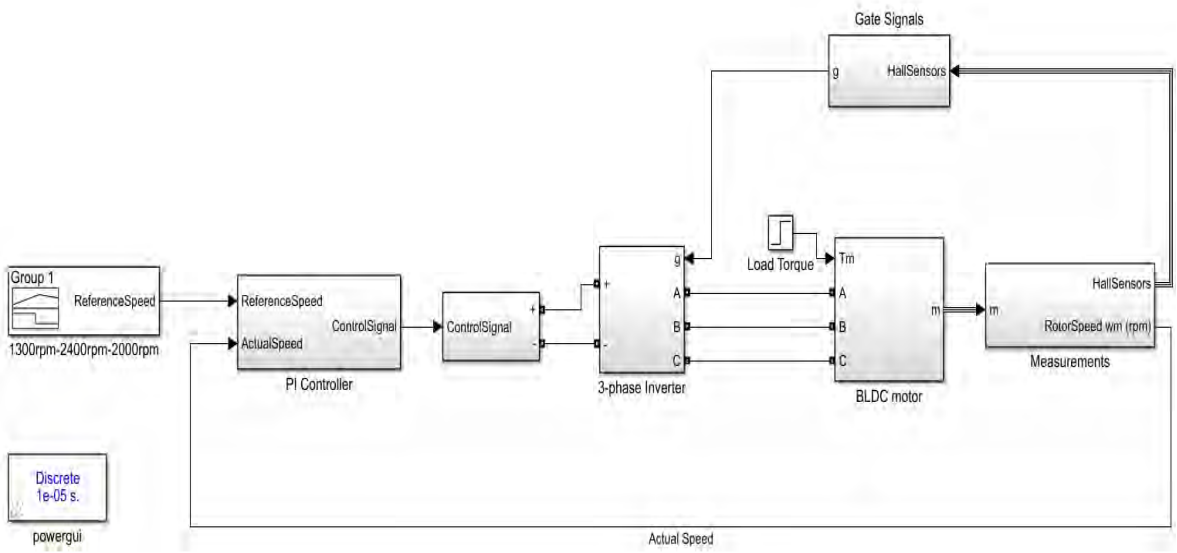

Figure 4.1 Complete Simulink/Matlab simulation model

This structure for closed loop control of BLDC motor consists of two control loops. One loop is responsible for energizing the correct switches at the inverter bridge depending on the hall sensor signals and the other loop regulates the motor's speed.

4.1.1 BLDC motor subsystem

In order to model the motor the block "Permanent Magnet Synchronous Motor" is used, shown in Figure 4.2, that is taken from library "SimPowerSystems" of Simulink. It is a

three-phase machine with trapezoidal back-EMF waveform. Its drive achieved through the three-phase voltage inverter. It has mechanical load as an input and its output is connected to the subsystem of measurements, which is shown in Figure 4.3. Motor measurement vector allows us to observe the motor's variables using the "Bus Selector" block.

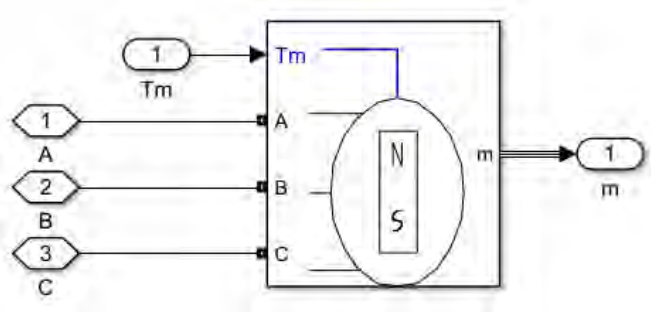

Figure 4.2 Motor model

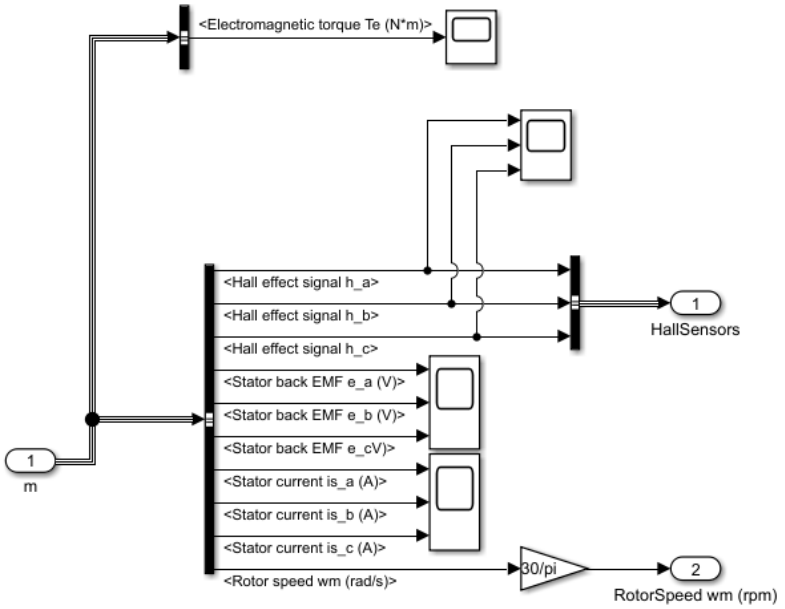

Figure 4.3 Measurements subsystem

4.1.2 Inverter subsystem

For the model of three-phase inverter is used the "Universal Bridge" block from library "SimPowerSystems" of Simulink. This block implements a universal three-phase power converter that consists of six power switches connected in a bridge configuration. For our

simulation model, MOSFET/Diodes power switch type is selected. Series RC circuits are connected in parallel with each switch device, with parameter values Rs=5000 Ohms and Cs=1µF.

The three-phase inverter is generated by DC voltage. The "Controlled Voltage Source" block converts the Simulink input signal, which comes from the PI controller, into an equivalent voltage source. The generated voltage is driven by PI controller's output control signal. The commutation of switches is regulated by Gate Signal subsystem.

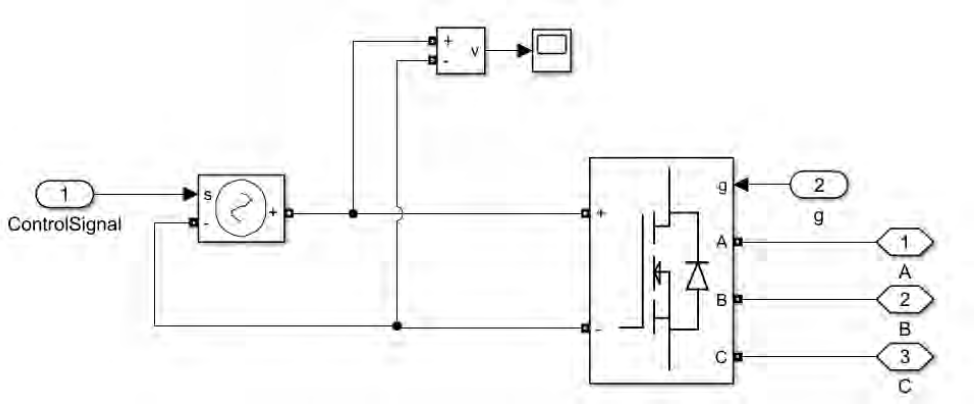

Figure 4.4 Inverter model

4.1.3 Gate Signal subsystem

This subsystem implements the decoding of Hall sensor signals by using the "Truth Table" block. This block outputs the signal sequence which is required to generate the appropriate switches, depending on the rotor's electrical angle (θ_e). Considering the inverter bridge configuration is similar to Figure 3.2, the decoding of Hall sensor signals is shown in Table 4.1.

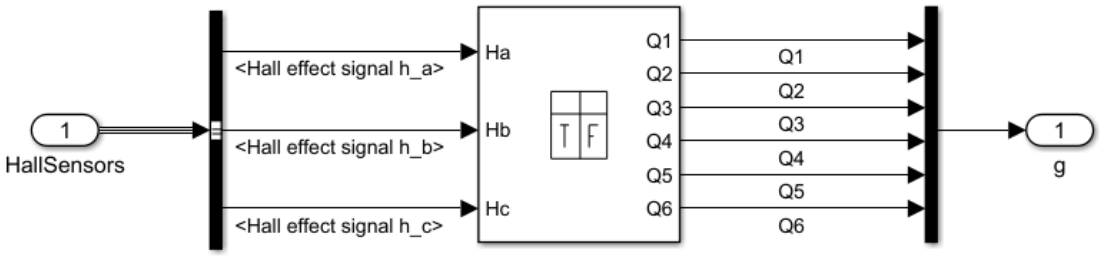

Figure 4.5 Gate signal subsystem

Table 4.1 Commutation sequence

$\boldsymbol{\theta_e}$	Sequence	Ha	Hb	Hc	Q1	Q2	Q3	Q4	Q5	Q6
0°-60°	1	1	0	1	1	0	0	1	0	0
60°-120°	2	1	0	0	1	0	0	0	0	1
120°-180°	3	1	1	0	0	0	1	0	0	1
180°-240°	4	0	1	0	0	1	1	0	0	0
240°-300°	5	0	1	1	0	1	0	0	1	0
300°-360°	6	0	0	1	0	0	0	1	1	0

4.1.4 PI Controller subsystem

In order to control the speed of the motor, PI controller system is implemented. As shown in Figure 4.6, the error difference between the actual speed and reference speed is given as an input to the controller. The controller outputs a control signal which is responsible for adjusting the voltage that is given to the inverter. The calculation of control signal is shown in Figure 4.7. In order to minimize the speed error, the controller is regulated by the appropriate proportional and integral gain, k_p and k_i.

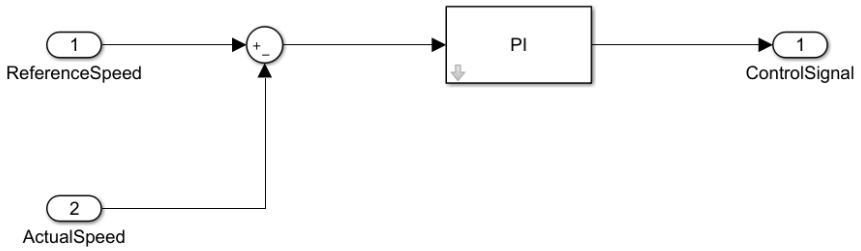

Figure 4.6 PI Controller subsystem

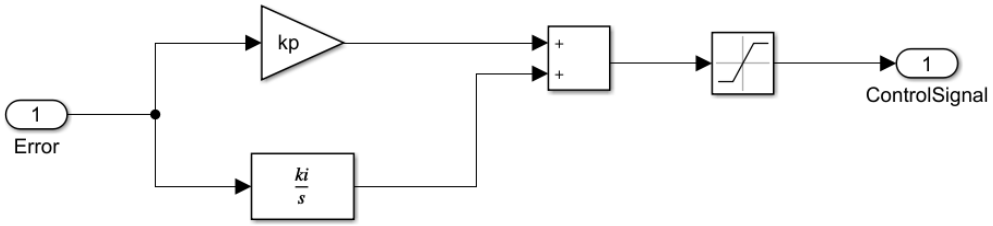

Figure 4.7 Subsystem of control signal calculation

CHAPTER 5

SIMULATION RESULTS

This chapter presents the simulation results of BLDC motor model in Simulink. The simulation is done by using the solver ode4 (Runge-Kutta) in configuration parameters settings and Table 5.1 displays the parameters that are given to the BLDC motor for simulation purposes. We set three consecutive reference speeds, 1300rpm-2400rpm-2000rpm, as input to our system and also we supply a load torque of 3 N_m at 0.2 seconds.

Table 5.1 BLDC motor parameters

Parameter	Symbol	Value	Unit
Stator phase resistance	R_s	2.8750	Ω
Stator phase inductance	L_s	$8.5 \cdot 10^{-3}$	H
Inertia	J	$0.8 \cdot 10^{-3}$	$kg \cdot m^2$
Damping constant	B	10^{-3}	$N \cdot m \cdot s$
Number of poles	P	4	poles

As far as the PI controller is concerned it is tuned by adjusting its tuning parameters (proportional gain, integral gain) in order to ensure the best response of the controller. The gains of PI are selected in such a way that the closed loop system has to give the desired response. The desired response should have minimal settling time with a small overshoot in the step response of the closed loop system. The integral term of the error eliminates steady-state error.

To optimize our system response, we give suitable values to PI parameters, based on Table 5.2. The setting values that are given to the controller for this simulation purpose are $K_p = 0.02$ and $K_i = 17$, corresponding to proportional gain and integral gain.

Table 5.2 PI controller parameter characteristics

Parameter increase	Rise time	Overshoot
K_p	Decrease	Increase
K_i	Decrease	Increase

The reference speed is modified by using the “Signal Builder” block, as shown in Figure 5.1.

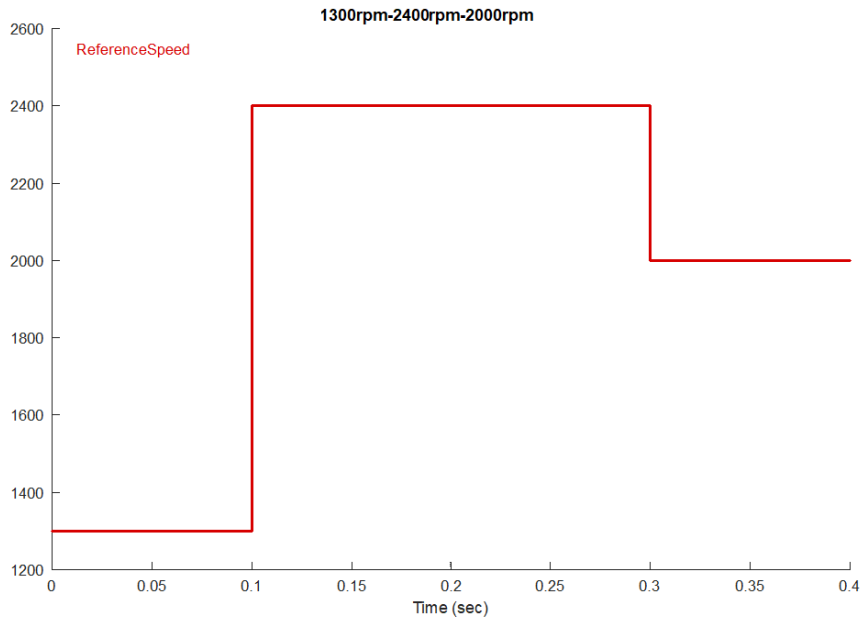

Figure 5.1 Reference speed

Figure 5.2 shows the rotor speed alteration in comparison with the reference speed. Starting the simulation, the reference speed is initialized to 1300rpm and the rise time is 0.038sec (38ms). When the reference speed is set to 2400rpm at 0.1 seconds, the rise time is increased at 0.073sec (73ms), because of the greater speed modification. Also, we observe that the overshoot is up to 1.67%. By applying a load torque at 0.2 seconds, the speed decays and then reaches 2400rpm with rise time 0.052sec (52ms). The final alteration occurs at 0.3 seconds by decreasing the speed to 2000rpm and the rise time is 0.046sec (46ms).

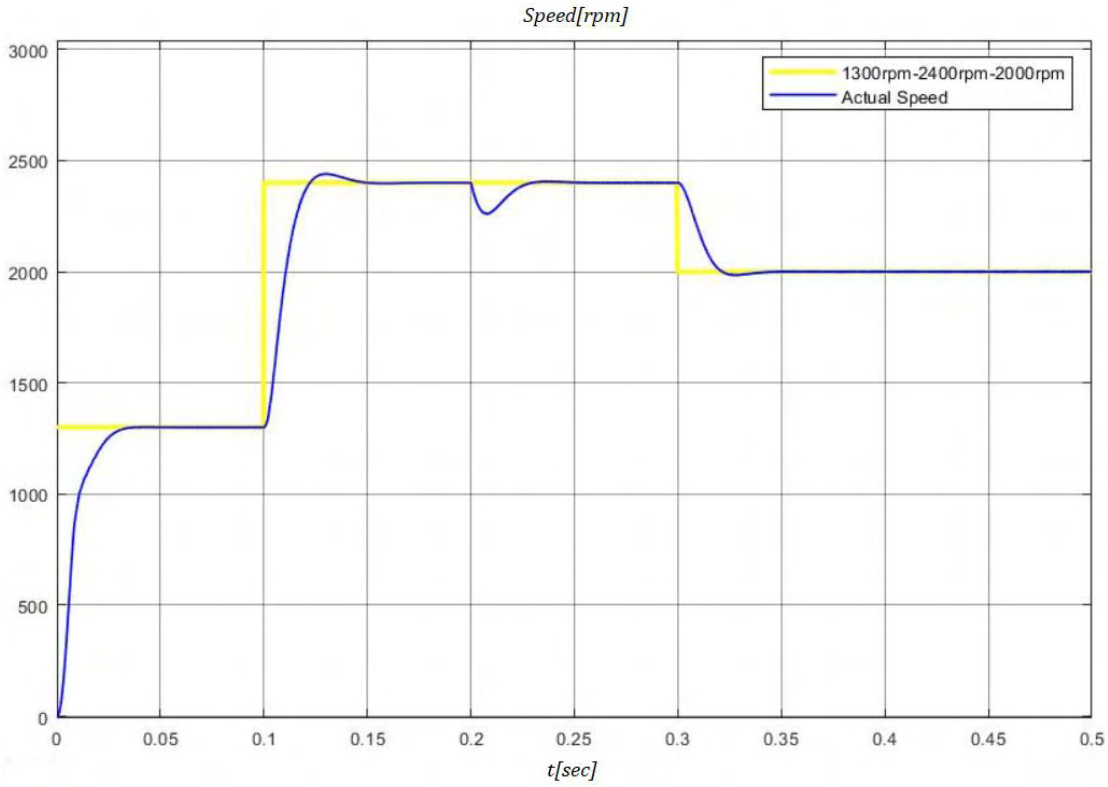

Figure 5.2 Reference speed - Actual speed

Figure 5.3 shows the rotor electromagnetic torque and Figure 5.4 shows the stator current alteration in association with the time. As we can observe in figures, the electromagnetic torque waveform is related to current waveform. Starting the simulation by setting speed to 1300rpm causes rapid increase of the electromagnetic torque. Also, the current starts with a high value and decays as the motor speeds up, until it reaches the target speed. We have similar response of torque waveform and current waveform by setting the reference speed to 2400rpm at 0.1 seconds.

By applying a load torque of 3 N_m at 0.2 seconds, the current rises again to hold the speed up to 2400rpm. Respectively, we observe increase of the generated electromagnetic torque.

After applying the load, we slow down the motor to 2000rpm at 0.3 seconds. A this time, we observe the decrease of the electromagnetic torque and the current for a period of time and then they increase again to maintain the speed up to 2000rpm synchronously with the applied load to the motor.

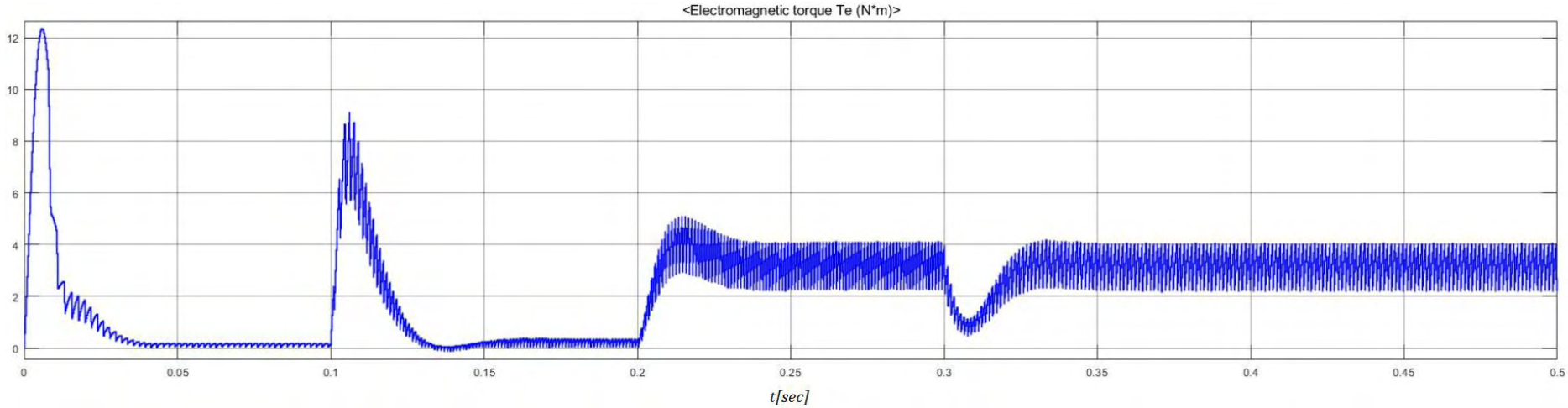

Figure 5.3 Electromagnetic torque waveform

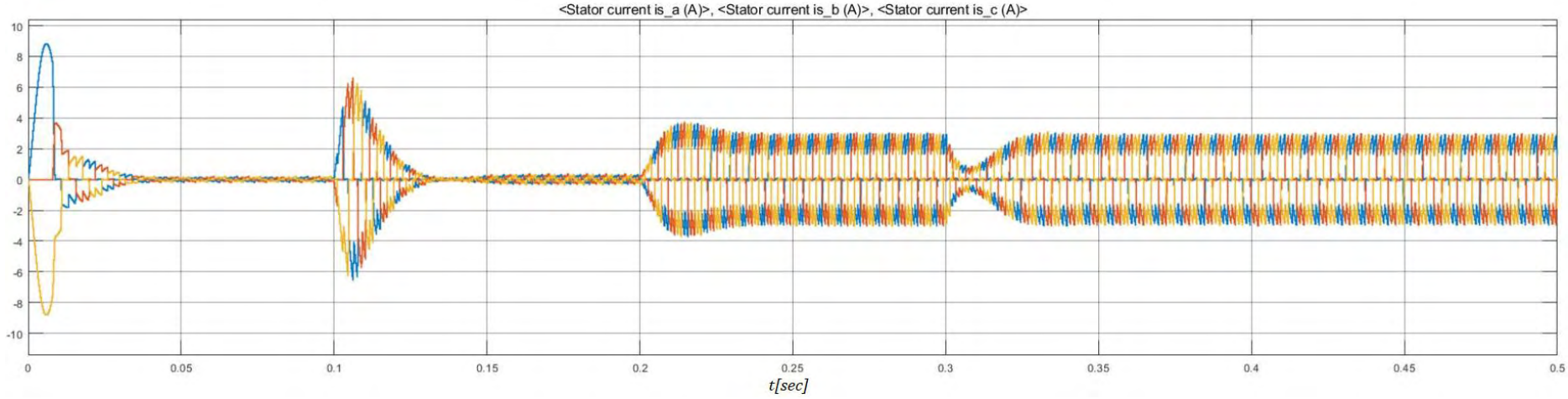

Figure 5.4 Stator currents waveform

Figure 5.5 shows the BEMF waveforms corresponding to the three stator windings and their alteration during speed change at 0.1sec and 0.3sec and the addition of mechanical load at 0.2sec.

Figure 5.5 Back-emf waveforms

Figure 5.6 shows the commutation sequence of the switches related to Hall sensor signals according to Table 4.1.

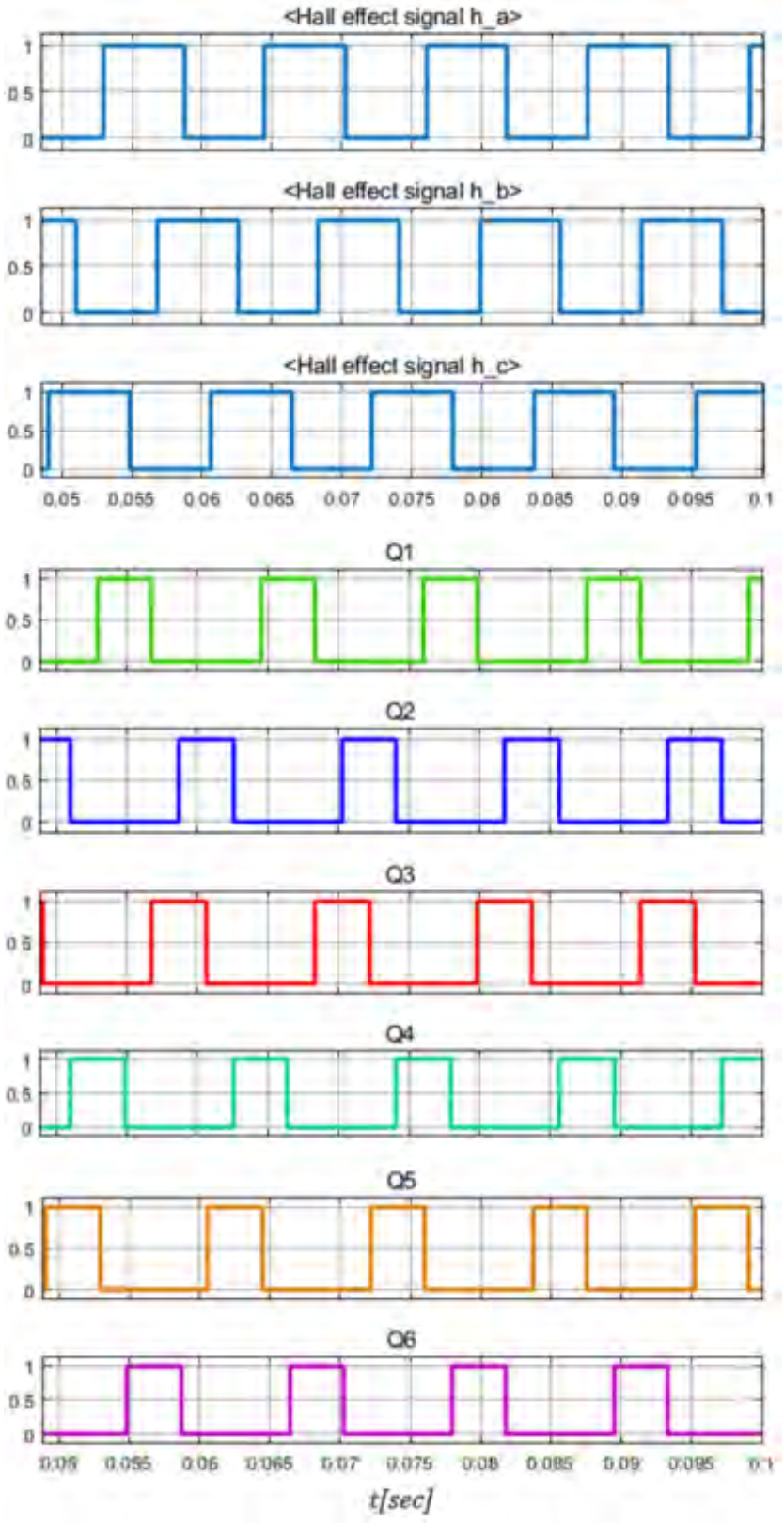

Figure 5.6 Hall sensor signals and commutation sequence

Figure 5.7 shows the Hall sensors related to the Back-EMF of the three phases.

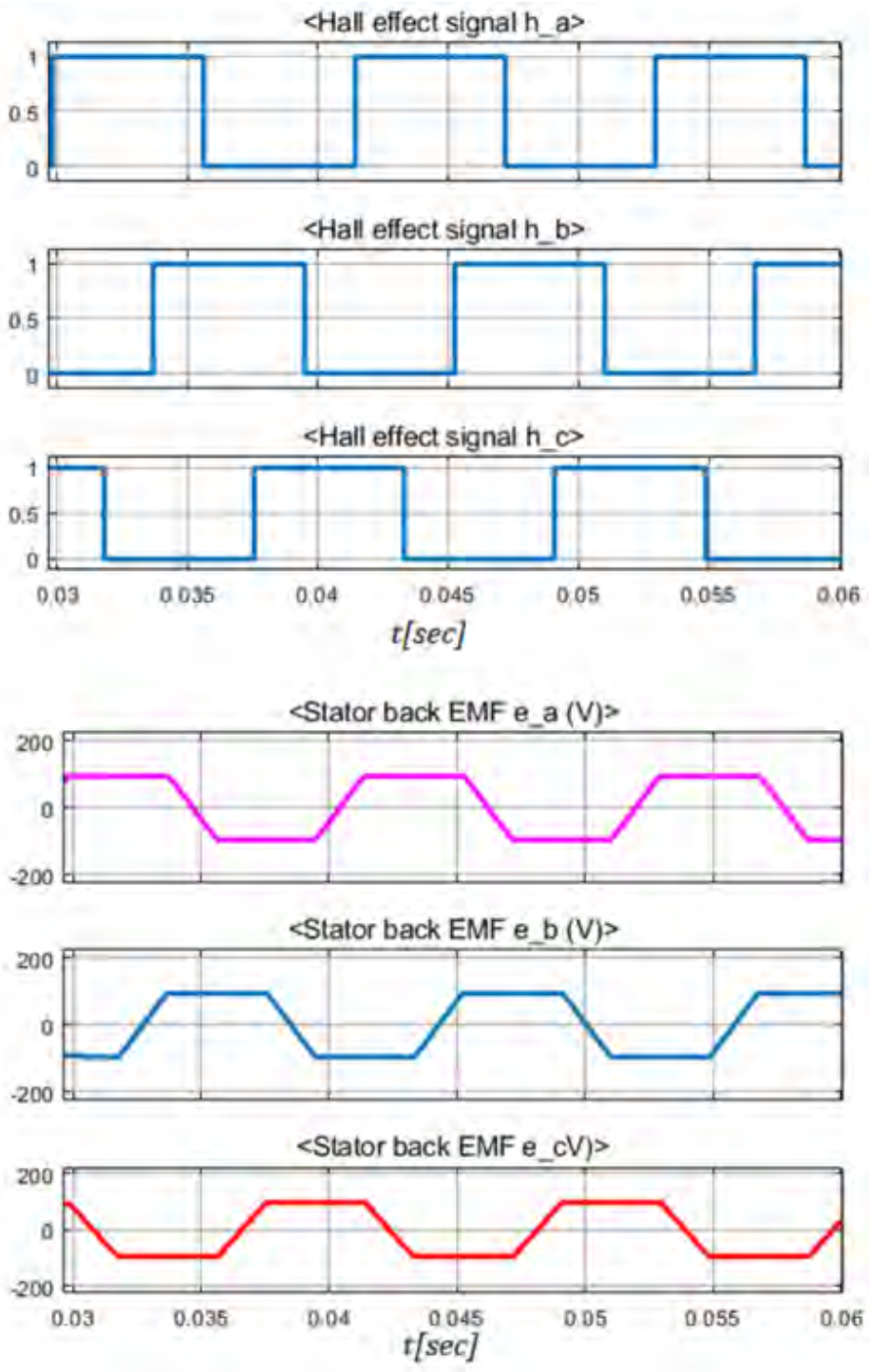

Figure 5.7 Hall sensor signals and BEMF

Figures 5.8 - 5.10 show the line voltages V_{ab} , V_{bc} and V_{ca} of the motor.

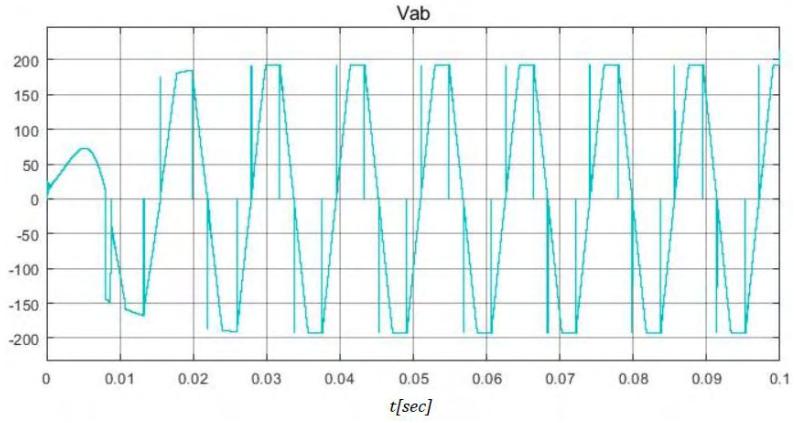

Figure 5.8 Line voltage Vab

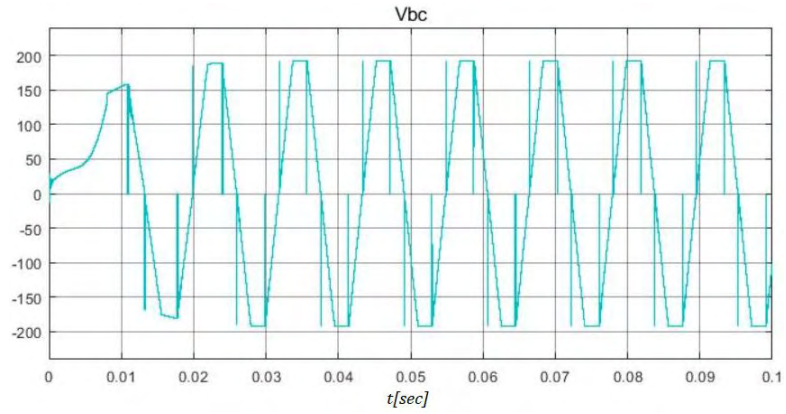

Figure 5.9 Line voltage Vbc

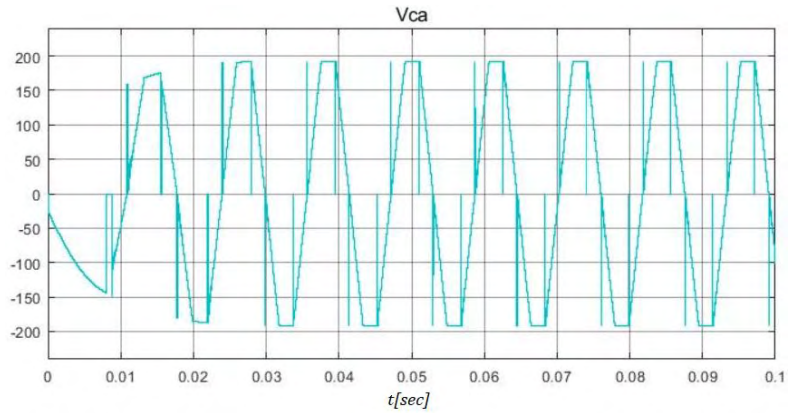

Figure 5.10 Line voltage Vca

Figures 5.11-5.13 show the relationship between Hall sensor signals, Back-EMFs and gate signals for phase A, phase B and phase C. The number of electrical cycles that must be completed to obtain a complete mechanical rotation is determined by rotor pole pairs. In every mechanical rotation there is one electrical cycle occurred for each pole pair. Therefore, for our motor model, which has two pole pairs, we observe 2 electrical cycles occurred in every mechanical rotation.

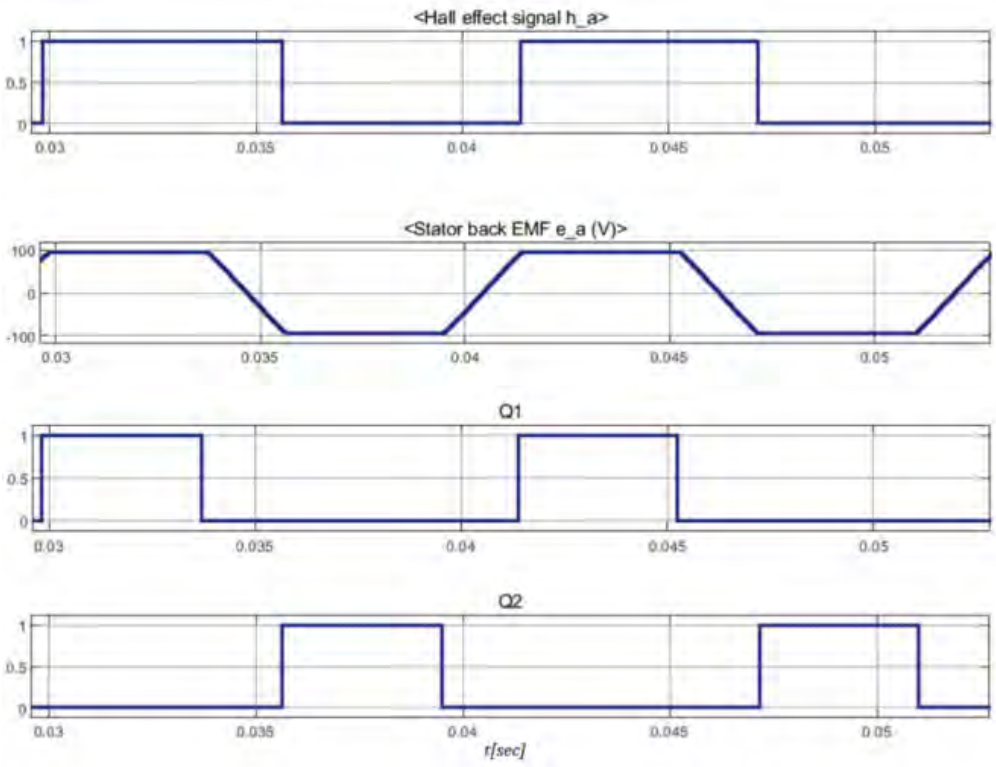

Figure 5.11 Relationship between Hall signal ha, BEMF, gate signal Q1, gate signal Q2 for phase A

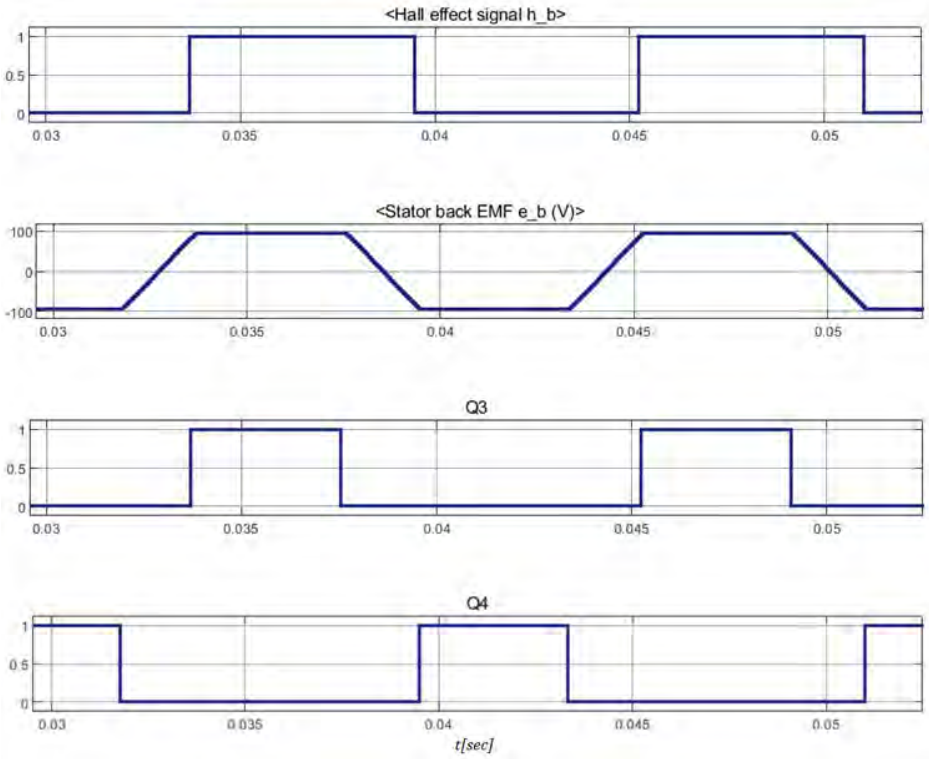

Figure 5.12 Relationship between Hall signal ha, BEMF, gate signal Q3, gate signal Q4 for phase B

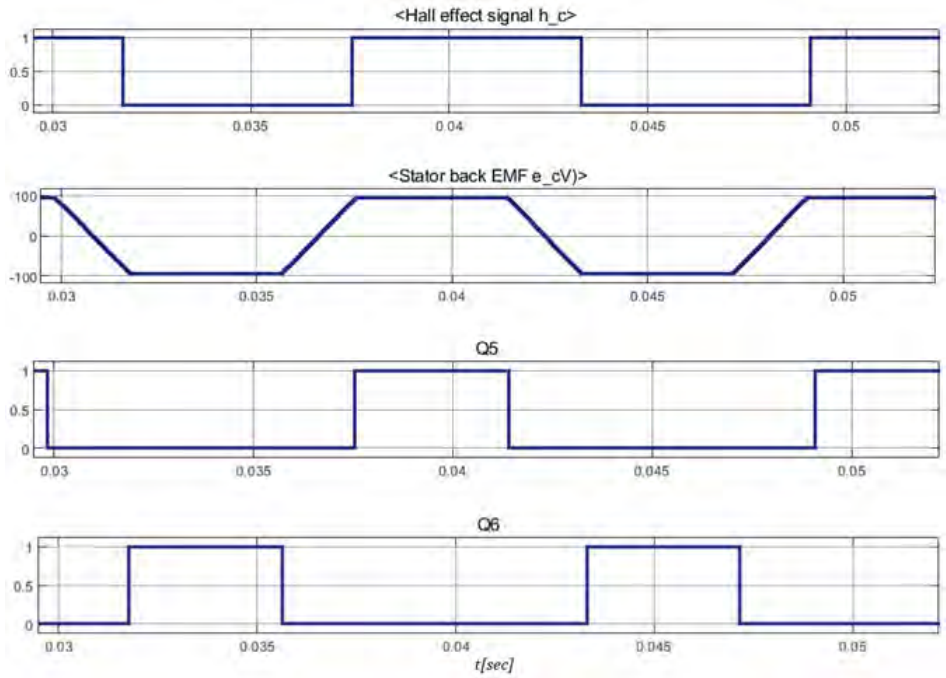

Figure 5.13 Relationship between Hall signal ha, BEMF, gate signal Q5, gate signal Q6 for phase C

CHAPTER 6

CONCLUSIONS

This thesis discusses the analysis of BLDC motor operation by analyzing its control systems. The implementation of motor model simulation occurs in Simulink/Matlab environment and, then, the simulation results are studied to observe the model reaction to speed alterations and mechanical load application. The response of the control system approaches the predicted results very sufficiently. BLDC motor proved to be not a complicated model, which can be easily modified by applying extra techniques to improve its operation.

A future work could be the implementation of motor drive system in a real BLDC motor and the comparison of the control system response with the simulation results. Also, we could replace the Hall sensor on this simulation model by implementing sensorless control methods and test their response. Moreover, the implemented simulation model of BLDC motor drive motor, with the required adjustment, could be utilized in an electric car simulation model.

BIBLIOGRAPFY

[1] V. Kiran and I.L.B.Sowjanya, "Speed Performance of a BLDC Motor Employing PWM/PAM Control Techniques," *International Journal of Application or Innovation in Engineering & Management ,* vol. 5, pp. 29-38, 2016.

[2] B. Alsayid, W. A. Salah and Y. Alawneh, "Modelling of sensored speed control of BLDC motor using MATLAB/SIMULINK," *International Journal of Electrical and Computer Engineering,* vol. 9, pp. 3333-3343, 2019.

[3] K. S. Patel and A.K.Pandey, "Modeling and Simulation of Brushless DC Motor Using PWM Control Technique," *International Journal of Engineering Research and,* vol. 3, pp. 612-620, 2013.

[4] G. Tatar, K. Toker, N. F. Oyman and H. Korkmaz, "A Dynamic Analysis of BLDC Motor by Using Matlab/Simulink and Mathematica," pp. 1-5, 2017.

[5] S. Lee, T. Lemley and G. Keohane, "A comparison study of the commutation methods for the three-phase permanent magnet brushless dc motor," 2009.

[6] Rao, P. A. Chandra, Y.p.Obulesh and S. Babu, "Mathematical modeling of BLDC motor with closed loop speed control using PID controller under various loading conditions.," vol. 7, pp. 1321-1328, 2012.

[7] Yadamale and Pandmaraya, *Brushless DC (BLDC) Motor Fundamentals,* Microchip Technology Inc , 2003.

[8] Momenzadeh, M. Mahdi, A. F. Ahmed and A. Tolba, "Modelling and simulation of the BLDC electric drive system using SIMULINK/MATLAB for a hybrid vehicle," 2014.

[9] K. Bhatt, S. Dhoranwala and A. Bosamiya, "Simulation of Brushless DC motor speed control in MATLAB," *International Journal of Advance Engineering and Research,* pp. 927-933, 2017.

[10] J. Jezny and M. Curilla, "Position Measurement with Hall Effect Sensors," *American Journal of Mechanical Engineering,* vol. 1, pp. 231-235, 2016.

[11] "https://www.electronics-tutorials.ws/category/electromagnetism," Electronics Tutorials, Hall Effect Sensor. [Online].

[12] S. Arumugam and C. Dinakaran, "Simulation and implementation of brushless DC motor using voltage source inverter with PIC16F877A," 2015.

[13] Mathew, Tony and C. A. Sam, "Closed Loop Control of BLDC Motor Using a Fuzzy Logic Controller and Single Current Sensor," *International Conference on Advanced Computing and Communication Systems,* pp. 1-6, 2013.

[14] P. Pal, T. M. Shubhum and A. Ojha, "Simulation of Brushless DC Motor for Performance Analysis using MATLAB/SIMULINK Environment," *International Journal on Recent and Innovation Trends in Computing and Communication,* vol. 2, pp. 1564-1567, 2014.

[15] T. Kim, C. Kim and J. Lyou, "A new sensorless drive scheme for a BLDC motor based on the terminal voltage difference," *IECON 2011 - 37th Annual Conference of the IEEE Industrial Electronics Society,* pp. 1710-1715, 2011.

[16] J. C. Gamazo-Real, E. Vázquez-Sánchez and J. Gómez-Gil, "Position and speed control of brushless DC motors using sensorless techniques and application trends," *Sensors,* vol. 10, pp. 6901-6947, 2010.

[17] G. Zacharia and A. Raina, "A Survey on Back EMF Sensing Methods for Sensorless Brushless DC Motor Drives," *International Journal of Emerging Trends in Engineering Research,* vol. 2, 2014.

[18] A. Mohammad, M. A. Abedin and Z. R. Khan, "Implementation of a three phase inverter for BLDC motor drive," *9th International Conference on Electrical and Computer Engineering,* pp. 337-340, 2016.

[19] S. J. Chapman, Electric Machinery Fundamental, 4th ed., TZIOLA, 2013.

[20] "https://www.electronics-tutorials.ws/transistor," Electronic Tutorials. [Online].

[21] G. K. Rao, M. V. Subramanyam and K. Satyaprasad, "Study on PID Controller Design and Performance Based on Tuning Techniques," *International Conference on Control,*

Instrumentation, Communication and Computational Technologies, 2014.

[22] A. Nayak and M. Singh, "Study of tuning of PID controller by using particle swarm optimization," *International Journal of Advanced Engineering Research and Studies,* pp. 346-350, 2015.

[23] R. Paz, "The Design of the PID Controller," *Klipsch School of Electrical and Computer Engineering,* 2001.